Article

Cell Reports

Structural and Functional Characterization of CRM1-Nup214 Interactions Reveals Multiple FG-Binding Sites Involved in Nuclear Export

Graphical Abstract

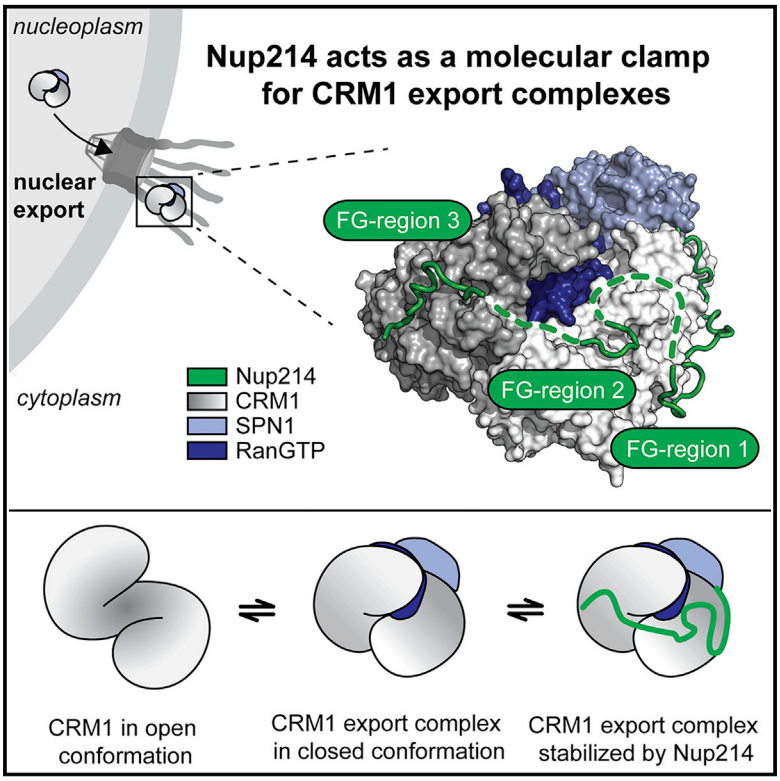

Highlights

- Crystal structure of a Nup214 fragment in complex with CRM1 reveals eight binding sites
- Nup214 FG motifs interact with CRM1 N- and C-terminal regions
- Nup214 stabilizes CRM1 in a closed conformation by acting as a molecular clamp

Authors

Sarah A. Port, Thomas Monecke, Achim Dickmanns, ..., Henning Urlaub, Ralf Ficner, Ralph H. Kehlenbach

Correspondence

rficner@uni-goettingen.de (R.F.), rkehlen@gwdg.de (R.H.K.)

In Brief

Port et al. present the crystal structure of an FG-repeat-containing fragment of Nup214, in complex with CRM1, SPN1, and RanGTP at 2.85 Å resolution. Nup214 FG motifs interact with CRM1 N- and C-terminal regions. Biochemical and cell-based data indicate that Nup214 stabilizes CRM1 by acting as a molecular clamp.

Accession Numbers

5DIS

Port et al., 2015, Cell Reports *13*, 690–702
October 27, 2015 ©2015 The Authors
http://dx.doi.org/10.1016/j.celrep.2015.09.042

OPEN ACCESS
CellPress

Cell Reports
Article

Structural and Functional Characterization of CRM1-Nup214 Interactions Reveals Multiple FG-Binding Sites Involved in Nuclear Export

Sarah A. Port,[1,5] Thomas Monecke,[2,5] Achim Dickmanns,[2] Christiane Spillner,[1] Romina Hofele,[3,4] Henning Urlaub,[3,4] Ralf Ficner,[2,*] and Ralph H. Kehlenbach[1,*]

[1]Department of Molecular Biology, Faculty of Medicine, GZMB, Georg-August-University Göttingen, Humboldtallee 23, 37073 Göttingen, Germany

[2]Department of Molecular Structural Biology, Institute for Microbiology and Genetics, GZMB, Georg-August-University Göttingen, Justus-von-Liebig-Weg 11, 37077 Göttingen, Germany

[3]Bioanalytical Mass Spectrometry Group, Max Planck Institute for Biophysical Chemistry, Am Fassberg 11, 37077 Göttingen, Germany

[4]Bioanalytics, Institute for Clinical Chemistry, University Medical Center, Robert-Koch-Str. 40, 37075 Göttingen, Germany

[5]Co-first author

*Correspondence: rficner@uni-goettingen.de (R.F.), rkehlen@gwdg.de (R.H.K.)

http://dx.doi.org/10.1016/j.celrep.2015.09.042

SUMMARY

CRM1 is the major nuclear export receptor. During translocation through the nuclear pore, transport complexes transiently interact with phenylalanine-glycine (FG) repeats of multiple nucleoporins. On the cytoplasmic side of the nuclear pore, CRM1 tightly interacts with the nucleoporin Nup214. Here, we present the crystal structure of a 117-amino-acid FG-repeat-containing fragment of Nup214, in complex with CRM1, Snurportin 1, and RanGTP at 2.85 Å resolution. The structure reveals eight binding sites for Nup214 FG motifs on CRM1, with intervening stretches that are loosely attached to the transport receptor. Nup214 binds to N- and C-terminal regions of CRM1, thereby clamping CRM1 in a closed conformation and stabilizing the export complex. The role of conserved hydrophobic pockets for the recognition of FG motifs was analyzed in biochemical and cell-based assays. Comparative studies with RanBP3 and Nup62 shed light on specificities of CRM1-nucleoporin binding, which serves as a paradigm for transport receptor-nucleoporin interactions.

INTRODUCTION

The nuclear pore complex (NPC) is a giant protein complex embedded between the inner and the outer nuclear membrane that allows transport of large proteins and ribonucleoprotein particles into and out of the nucleus. At the same time, it restricts translocation by diffusion of small proteins and, thus, functions as a selective gate (Cook et al., 2007; Wente and Rout, 2010). The majority of actively translocated proteins interact with receptor proteins of the importin β superfamily, also referred to as karyopherins or importins/exportins. They mediate the translocation by binding to nucleoporins (Nups), the proteins forming the NPC. Another common binding partner of all karyopherins is the GTPase Ran. In nuclear import, binding of RanGTP to the importin results in dissociation of the import complex in the nucleus and to its release from a nucleoporin-binding site. In nuclear export, RanGTP is part of the export complex and accompanies it to the cytoplasmic side of the NPC. With RanGTP and nucleoporins as common binding partners, importins and exportins share many structural features. Generally, karyopherins are characterized by a modular architecture with a variable number of tandem HEAT repeats. Each HEAT repeat consists of two antiparallel α helices (A and B helix), connected by a short loop (Cook et al., 2007).

Common to all models for nuclear transport is the binding of importins/exportins to FG repeats found in about a third of the ~30 nucleoporins, the so-called FG-Nups (Iovine et al., 1995; Rexach and Blobel, 1995); for review, see Grossman et al. (2012), Stewart (2007), and Terry and Wente (2009). FG-Nups in general are important for NPC function (Strawn et al., 2004), and FG-Nups that delineate the transport channel play important roles in the formation of the permeability barrier of the NPC (Hülsmann et al., 2012). FG-Nups located at the cytoplasmic filaments of the NPC were suggested as initial or terminal binding sites for transport complexes (Kehlenbach et al., 1999; Yokoyama et al., 1995).

The best-characterized transport receptor with respect to FG-Nup binding is importin β (Chi et al., 1997; Kose et al., 1997; Kutay et al., 1997). Crystal structures of an importin β fragment with FG peptides revealed a hydrophobic interaction of the peptides with the outer surface of the N-terminal region of importin β (Bayliss et al., 2000, 2002; Liu and Stewart, 2005). A second nucleoporin-binding site was identified in the C-terminal half of importin β. Molecular dynamics simulations suggested that many more nucleoporin interaction sites are present in importin β (Isgro and Schulten, 2005) and probably in other transport receptors as well. Crystal structures of transport receptors showing multiple

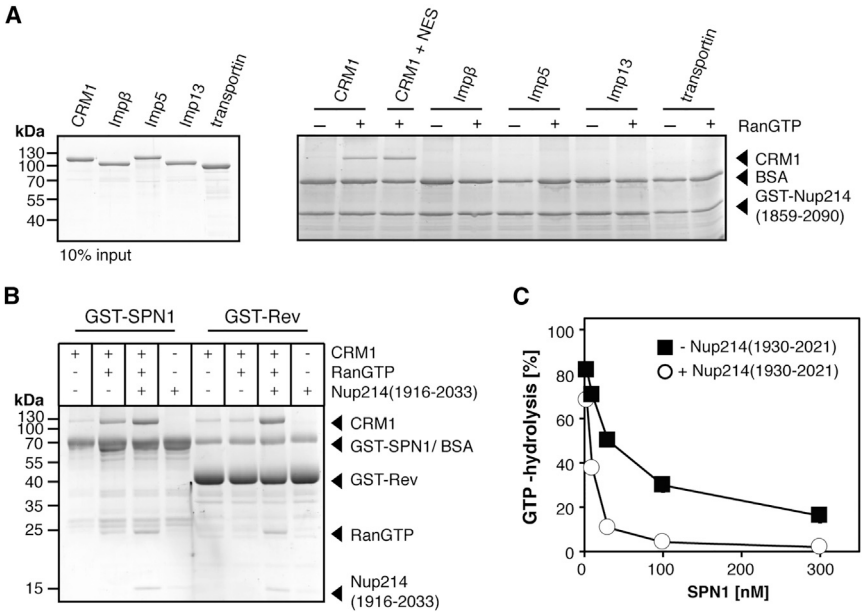

Figure 1. Nup214 Stabilizes CRM1 Export Complexes

(A) 50 pmol GST-Nup214$_{1,859–2,090}$ was immobilized on glutathione beads and incubated with 50 pmol of CRM1, importin β, importin 5, importin 13, or transportin in the absence or presence of 375 nM RanGTP$_{Q69L}$ and, for CRM1, 2.5 μM NES peptide. Bound proteins were analyzed by SDS-PAGE, followed by Coomassie staining.

(B) 500 pmol of GST-SPN1 or GST-HIV-1 Rev (GST-Rev) was immobilized on glutathione beads and incubated with or without 250 pmol CRM1, RanGTP$_{Q69L}$, and His-Nup214$_{1,916–2,033}$ as indicated. Bound proteins were analyzed by SDS-PAGE, followed by Coomassie staining.

(C) RanGAP assays were performed with increasing concentrations of SPN1 in the absence or presence of 3 μM MBP-Nup214$_{1,930–2,021}$. All reactions contained 500 nM CRM1. The mean of three independent experiments is shown. Error bars are too small to be seen.

interactions with nucleoporins, however, are not available so far. FG-rich regions of nucleoporins are usually not resolved in crystal structures, most likely because they tend to be natively unfolded (Denning et al., 2003) and may only adopt a defined structure upon interaction with a binding partner.

CRM1 is the most-prominent nuclear export receptor (Fornerod et al., 1997a; Fukuda et al., 1997; Kehlenbach et al., 1998; Ossareh-Nazari et al., 1997). It transports hundreds of different proteins harboring nuclear export signals (NESs) out of the nucleus and is also a major factor in RNA export (Hutten and Kehlenbach, 2007). CRM1 consists of an array of 21 HEAT repeats and adopts an overall pitched and superhelical conformation in its free form (Monecke et al., 2013). Cargo and/or RanGTP-bound CRM1 changes its conformation toward a closed ring-like or toroidal shape, where the N- and C-terminal arches interact (Dong et al., 2009a, b; Güttler et al., 2010; Monecke et al., 2009). CRM1 binds RanGTP on the interior with major contributions of N-terminal HEAT repeats 1–6 (H1–6) in addition to residues of the acidic loop, a long β-hairpin in H9 (Monecke et al., 2009). In contrast, the cargo SPN1 is bound on the outer surface and interacts with CRM1 via the N-terminal NES, the central cap-binding domain, and the C-terminal 12 residues (Dong et al., 2009b; Monecke et al., 2009).

Formation of the export complex in the nucleus is a rate-limiting step in nuclear export (Kehlenbach et al., 2001), and several factors have been identified that promote the formation of CRM1-containing complexes. The best-characterized factor is the Ran-binding protein RanBP3 (Yrb2p in yeast), which binds directly to CRM1 and enhances its affinity for RanGTP and for NES cargoes (Englmeier et al., 2001; Lindsay et al., 2001). Similar effects have been suggested for the nucleoporins Nup98 (Oka et al., 2010) and NLP1/hCG1 (Waldmann et al., 2012). The nucleoporin with the highest affinity for CRM1 is Nup214 (von Lindern et al., 1990), which localizes to the cytoplasmic side of the NPC (Panté et al., 1994). An FG repeat region within the C terminus of Nup214 is required for its interaction with CRM1 (Fornerod et al., 1996, 1997b), and several FG motifs contribute to efficient binding (Roloff et al., 2013).

CRM1 binding to Nup214 is promoted by RanGTP (Kehlenbach et al., 1999), suggesting that the nucleoporin is involved in a late step of nuclear export. Depletion of Nup214 resulted in inhibition of nuclear export of some, but not all, CRM1-dependent cargoes (Bernad et al., 2006; Hutten and Kehlenbach, 2006). Nup214 stabilizes the interaction between the export receptor, RanGTP, and the transport cargo (Hutten and Kehlenbach, 2006), although the significance of this effect of a cytoplasmic nucleoporin remains unclear.

In this study, we solved the structure of the CRM1 export complex binding a 117-amino-acid fragment of the FG repeat region of Nup214 by X-ray crystallography. Structural data were corroborated by means of mass spectrometry, and site-directed mutagenesis studies unraveled the contribution of individual FG repeats to CRM1 binding in cell-based and in vitro assays. Our data provide insights into the interaction of karyopherins and nucleoporins during nucleocytoplasmic transport.

RESULTS

Interaction of CRM1 and Nuclear Export Complexes with Nup214

We showed that several FG repeats in the C-terminal region of Nup214 are involved in CRM1 binding (Roloff et al., 2013), confirming and extending previous results (Fornerod et al., 1997b). To gain insight into binding specificities, we immobilized an FG-repeat-containing C-terminal fragment of Nup214$_{1,859–2,090}$ fused to GST and tested binding of CRM1, importin β, importin 5, importin 13, and transportin. Significant binding of CRM1 to Nup214 was observed in the presence, but not in the absence, of RanGTP (Figure 1A). Binding was increased by the addition of an NES peptide, as shown before (Hutten and Kehlenbach,

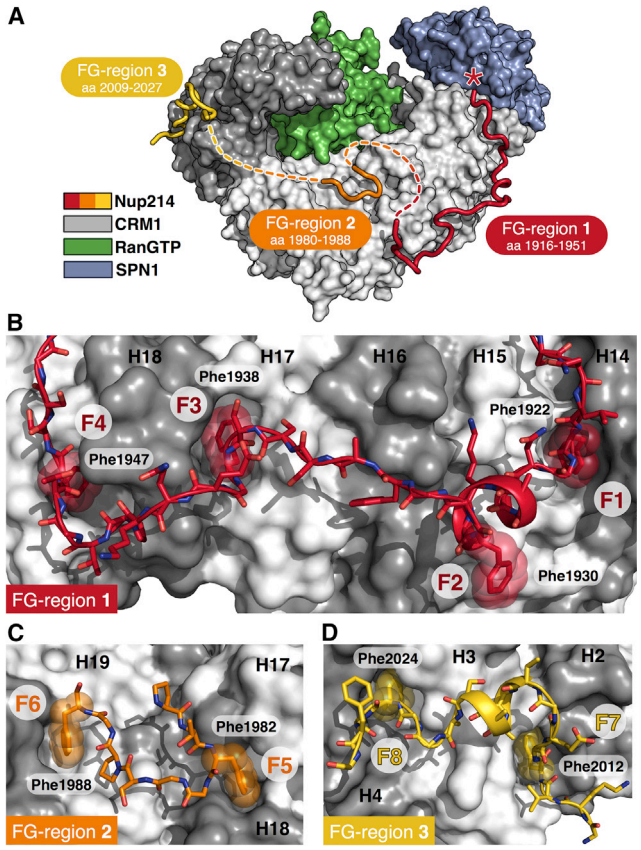

Figure 2. Architecture of the CRM1-SPN1-RanGTP-$_{MBP}$Nup214 Complex

(A) Overall structure of the Nup214 export complex. Three FG regions of Nup214 (red, orange, and yellow) bind to three distinct, mainly hydrophobic FG-binding patches on CRM1 (gray-white-gradient-colored surface from N to C terminus). RanGTP (green) is engulfed by the N-terminal region, the acidic loop, and C-terminal HEAT repeats of CRM1. SPN1 (blue) binds to the outer surface of CRM1 via two epitopes: the NES residues and the cap-binding domain. MBP, which was fused to the N terminus of Nup214 for crystallization, was omitted for clarity. It is located in front of SPN1, preceding the FG region 1 (indicated by a red asterisk; compare Figure S2A).

(B–D) Detailed views of FG region 1 (red), FG region 2 (orange), and FG region 3 (yellow) of Nup214 bound to the respective FG-binding patches of CRM1. HEAT repeats are labeled and colored alternately in gray and white. Nup214 is shown in cartoon mode and as sticks. Phenylalanines of the FG repeats are illustrated by transparent spheres and labeled.

See also Figures S2–S4 and Table S1.

2006; Roloff et al., 2013). Other transport receptors did not interact with Nup214 under these conditions.

In a complementary approach, we immobilized the CRM1 cargoes SPN1 and HIV-1 Rev and analyzed binding of CRM1 and RanGTP in the absence or presence of a Nup214 fragment. The addition of a Nup214 fragment enhanced binding of CRM1 and RanGTP to GST-SPN1 (Figure 1B). This effect was even more pronounced for GST-HIV-1 Rev, where CRM1- and Ran-binding was only observed in the presence of the Nup214 fragment (Figure 1B).

Using RanGAP assays, we previously showed that CRM1 interacts with Nup214 fragments (Hutten and Kehlenbach, 2006; Roloff et al., 2013). This assay is based on the observation that RanGTP in a complex with a transport receptor is largely insensitive to the GTPase-stimulating activity of RanGAP (Floer and Blobel, 1996; Görlich et al., 1996). We now used it for a quantitative analysis of the effect of Nup214 fragments on export complex formation. In the presence of a limiting concentration of a Nup214$_{1,930–2,021}$ fragment, which on its own resulted only in a moderate protection from RanGAP-induced GTP hydrolysis, the two CRM1 cargoes SPN1 (Figure 1C) and the NES peptide (data not shown) were much more efficient in reducing RanGTP hydrolysis and thus stable export complex formation. Strikingly, full protection of the export complex from GTP hydrolysis was only observed in the presence of the Nup214 fragment. In light of the tight and specific interaction of Nup214 and CRM1, this complex appeared particularly suitable for structural analysis.

Complex Assembly, Crystallization, and Structure Determination

To gain insight into the structural details of the Nup214-CRM1 interaction, we co-crystallized the CRM1-RanGTP-SPN1 complex with a Nup214 fragment comprising amino acids 1,916–2,033 (Nup214$_{1,916–2,033}$). This fragment containing 12 FG motifs was fused to the C terminus of MBP. The C-terminal deletions RanGTP$_{1–180, Q69L}$ and SPN1$_{1–291}$ were used for complex formation. The purified components were mixed, and the resulting CRM1-SPN1-RanGTP-$_{MBP}$Nup214 complex was purified by gel filtration (Figures S1A and S1B) and subjected to crystallization trials. The complex crystallized in PEG8000 conditions, yielding crystals belonging to space group $C222_1$ that contain one quaternary complex in the asymmetric unit (Table S1). The diffraction properties of initial crystals (Figure S1C) could be significantly improved by dehydration and post-mounting optimization steps. The crystal structure was solved by means of molecular replacement using the ternary CRM1-SPN1-RanGTP complex (PDB: 3GJX) as search model and refined at a resolution of 2.85 Å. For the final model, residues 5–388 and 401–1,048 of CRM1; residues 1–28, 32–73, 93-162, and 166-287 of SPN1; residues 8–179 of RanGTP; and Nup214 residues 1,916–1,951, 1,980–1,988, and 2,009–2,027 were placed in the electron density map.

Overall Structure of the CRM1-SPN1-RanGTP-$_{MBP}$Nup214 Complex

The overall conformation and interaction pattern of CRM1, RanGTP, and SPN1 in the complex is essentially unaltered compared to the crystal structure of the ternary complex (PDB: 3GJX). CRM1, RanGTP, and SPN1 superpose with root-mean-square deviations (rmsds) of 0.68 Å (for 975 common C_α atoms), 0.33 Å (for 171 common C_α atoms), and 0.57 Å (for 248 common C_α atoms), respectively. CRM1 adopts a closed, ring-like conformation and binds RanGTP via several regions including the N-terminal six HEAT repeats, the acidic loop, as well as H17 and 19 (Figure 2A). SPN1 binds to the outer surface of H11–14 via two epitopes: the NES and the cap-binding domain. Because truncated SPN1 lacking the C-terminal 69 amino acids was used, the C-terminal 12 residues of SPN1 representing the third CRM1-binding epitope, which are in contact with HEAT repeats 14–16 in the ternary complex structure (PDB: 3GJX), are missing.

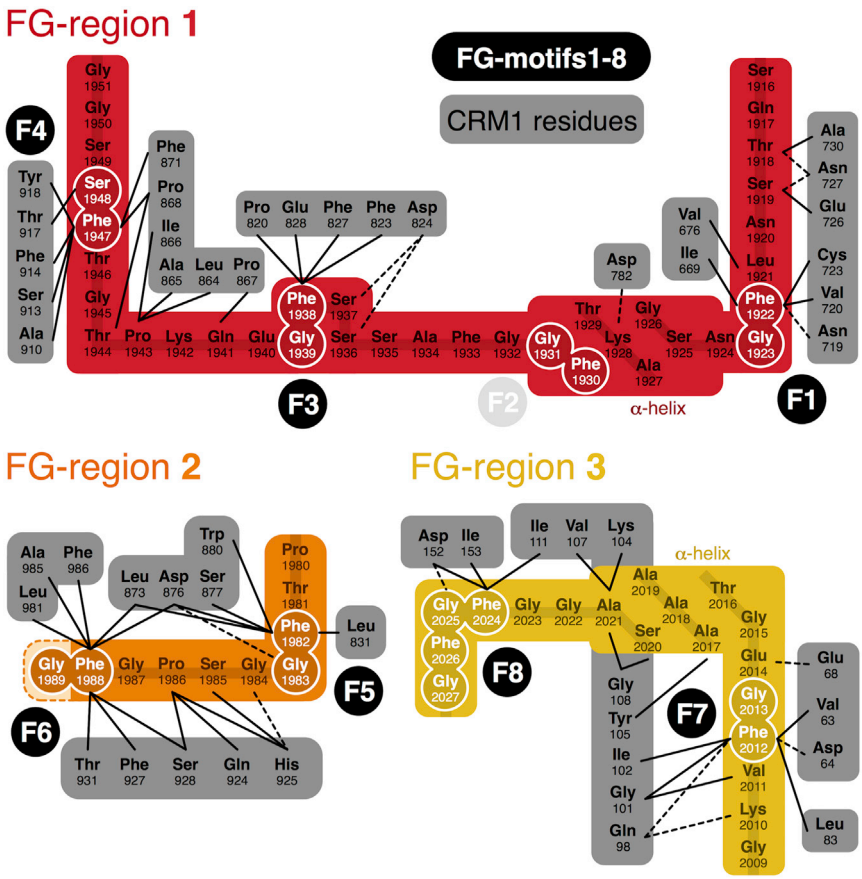

Figure 3. Schematic Representation of Interactions between Nup214 and CRM1

Nup214 is depicted in red (FG region 1), orange (FG region 2), or yellow (FG region 3). Interacting CRM1 residues are depicted as gray boxes representing individual HEAT repeats. Polar interactions are represented as dashed lines (≤3.5 Å), whereas hydrophobic and van-der-Waals interactions are depicted as solid lines (≤4 Å). FG motifs (F1–F8; for F2 see also Figure S4) are encircled in white and highlighted, and α-helical regions of Nup214 are labeled. See also Figures S4 and S5 and Tables S2 and S3.

Electron density corresponding to the fused MBP was found between two symmetry-related CRM1 complexes. MBP contacts H15 of one CRM1 molecule and several HEAT repeats including H10–12 and H15–16 of another. The C-terminal amino acids of MBP, the connecting linker peptide, and the N-terminal residues of the Nup214 fragment are located next to H14A and 15A.

The Nup214 fragment winds around the outer, convex surface of CRM1 (Figure 2A). FG motifs represent the prominent anchor points in the Nup214 chain, as they are well defined in the electron density (Figure S2). Conversely, the intervening sequences between FG motifs are only loosely attached to the CRM1 surface and thus show weaker densities and elevated B factors compared to the FG residues. In general, phenylalanine side chains of Nup214 FG motifs neatly dock into hydrophobic surface pockets of CRM1, which are formed by hydrophobic side chains of amino acid residues of neighboring HEAT helices. Some of these hydrophobic surface pockets have also been identified in CRM1 structures lacking FG-binding partners, as discussed later.

Overall, three major FG-binding patches (1–3) are found on CRM1 that interact with defined FG regions of Nup214 (Figure 2A). Residues connecting these three Nup214 FG regions are not defined in the electron density map (indicated by dashed lines in Figure 2A). The linkers between the Nup214 fragments are long enough to connect the three regions, and thus, it is likely that all patches derive from the same Nup214 chain. However, we cannot completely exclude the possibility that symmetry-related Nup214 molecules are involved as well.

FG region 1 contains four canonical FG motifs named F1–F4, whereas FG region 2 contains only two FG motifs (F5 and F6; Figures 2B and 2C). FG region 3 includes one FG motif (F7) and one FGFG motif (F8; Figure 2D). The FG-binding pockets on CRM1 are correspondingly termed P1–P8. FG-binding patch 1 on CRM1 is located on the surface of H14–19, corresponding to a total surface on CRM1 of 1,374 Å^2 (Figure 2B). In this region, 36 residues (Ser1916-Gly1951) of Nup214 are bound, including the FG motifs F1, F3, and F4. Ser1919^{Nup214} forms a hydrogen bond to the side chain of Asn727^{CRM1}, bridging a distance of 2.8 Å and anchoring the N-terminal portion of the Nup214 chain on CRM1. Phe1922^{Nup214}, which belongs to F1, is buried in the hydrophobic pocket P1 formed by the CRM1 residues Ile669, Ala672, Thr673, Val676, and Leu679 of H14 as well as Asn719, Val720, and Cys723 of H15 (Figure 3). Interestingly, this interaction site overlaps with the binding site for the C-terminal residues of SPN1 as observed for the ternary CRM1-RanGTP-SPN1 complex (Figure S3). Cys356^{SPN1} in the ternary complex, for example, partially occupies the space of Phe1922^{Nup214} in this complex, suggesting that these two regions may bind to CRM1 in a mutually exclusive manner.

Adjacent to Phe1922^{Nup214}, amino acids 1,924–1,928 of Nup214 describe a helical turn, at the end of which Phe1930^{Nup214} of F2 binds in a shallow hydrophobic groove (P2) formed by Asn30, Val31, Cys34, Gln42, Ala46, and Val49 of H1 and Ala12 of the N-terminal helix (Met5-Asp18) of a symmetry-related CRM1 molecule (Figure S4). Because F2 mediates crystal contacts, the local structure of Nup214 could be influenced by the interaction with the symmetry-related molecule. Interestingly, this N-terminal helix of CRM1 has so far only been defined in crystal structures where the N terminus is involved in crystal contacts. Consequently, this binding site at the N-terminal tip of CRM1 as well as the whole FG-binding patch 1 has not been observed in the recently described crystal

structure of the yeast CRM1-RanGTP-RanBP3 complex (Koyama et al., 2014; PDB: 3WYF). Next, Nup214 spans the outer helices 15A–17A. The four residues ^{1,937}SFGE^{1,940} describe a pitched β turn, exhibiting two prominent kinks (Figure 2B). In this turn, Phe1938^{Nup214} of F3 is located at one of the kinks, and this prominent position enables the phenyl group to insert deeply into a hydrophobic pocket (P3) located between helices 17A (Pro820, Phe823, Asp824, Phe827, and Glu828) and 18A (Ile866, Pro867, and Gln870; Figures 2B and 3).

The following Nup214 residues (1,941–1,944) cross the loop between HEAT repeat helices 18A and 18B (e.g., the base of H18). After an additional turn, the chain follows the groove between the A helices of H18 and 19. Here, Phe1947^{Nup214} of F4 deeply inserts into P4 between these two HEAT repeats and closely interacts with CRM1 residues Pro868 and Phe871 (H18) and Ala910, Ser913, Phe914, Thr917, and Tyr918 (H19) that are part of the hydrophobic core formed by these four helices.

FG-binding patch 2 involves H17–20 (Figures 2A and 2C). A stretch of nine Nup214 amino acids (residues Pro1980-Phe1988) containing F5 and F6 (FG region 2) buries a total surface of 481 Å^2 on CRM1 (Figure 2C). Phe1982^{Nup214} is bound in a rather shallow groove between HEAT repeats 17 (Leu831) and 18 (Leu873, Asp876, Ser877, and Trp880; Figure 3). Binding of the Nup214 residues Phe1982 and Gly1983 (F5) to P5 of CRM1 results in a sharp kink representing a β turn, which is characterized by a hydrogen bond between the main chain carbonyl of Thr1981^{Nup214} and the main chain amide of Gly1984 ^{Nup214}. Phe1988^{Nup214} of the adjacent F6 is positioned between H19 (Gln924, Phe927, Ser928, and Thr931) and H20, interacting with residues Leu981, Ala985, and Phe986.

FG-binding patch 3 on CRM1 is formed by the N-terminal H2–4 (754 Å^2 buried surface on CRM1; Figures 2A and 2D). The corresponding FG region 3 on Nup214 encompasses 19 residues (Gly2009-Gly2027) and comprises F7 and F8. It contacts the groove between H2A and 3A with Phe2012^{Nup214} sticking in a hydrophobic pocket (P7) formed by Trp60, Val63, and Asp64 of H2A as well as Gln98, Gly101, Ile102, and Tyr105 of H3A (Figures 2D and 3). Usually, the hydrophobic pockets on the surface of CRM1 are formed by the A helices of the respective HEAT repeats. Interestingly, in P7, Leu83, located in helix H2B, also contributes to the pocket, reflecting its profound depth. Next, an adjacent α-helical segment, which orthogonally crosses H3, causes a 90° kink in the Nup214 chain (Figure 2D). After an additional kink, Phe2024^{Nup214} (F8) inserts into FG-binding pocket P8 between H3 (Val107, Ile111 of helix 3A, and Leu134 of helix 3B) and H4 (Phe149, Asp152, and Ile153 of helix 4A and Ile134, Ile170, Asn167, and Leu163 of helix 4B).

To determine whether the FG pockets on CRM1 are formed in the absence of Nup214 or induced by binding of FG motifs, we compared the crystal structure of CRM1-RanGTP-SPN1-Nup214 to those of the ternary CRM1-RanGTP-SPN1 (PDB: 3GJX) complex and free CRM1 (PDB: 4FGV). In the CRM1-RanGTP-SPN1 complex, all pockets are found as in the bound state and thus are preformed with the exception of P3, which is locked by the side chain of Gln870. In contrast, only two pockets (P5 and P8) are entirely present in free CRM1, whereas P1 and P4 are principally preformed, but amino acid stretches preceding or following the Nup214 FG motifs (Phe1947-Ser1948 for F4 and Ser1916-Asn1920 for F1) would clash with the CRM1 surface. P3 is occluded by Gln867, which protrudes deeply into the pocket. Furthermore, P6 is locked by Phe927, which is not conserved in metazoan CRM1. Finally, P7 is occluded by Trp40 in free CRM1 and narrower in the CRM1-RanGTP-SPN1 complex (Trp60). Together, adjustments within the CRM1 structure upon binding of RanGTP and cargo seem to prepare the export receptor for nucleoporin binding, which is further optimized upon first contact with an FG repeat.

To confirm that the crystal structure is consistent with protein-protein interactions that occur in solution, we performed crosslinking experiments with the tetrameric CRM1-RanGTP-SPN1-Nup214$_{1,916–2,033}$ complex, using BS3 as a lysine-reactive reagent. Crosslinking sites were identified by mass spectrometry, and the intra- and intermolecular crosslinking distances were compared with the 3D structure of the C-terminal Nup214 fragment bound to the export complex. These analyses revealed 51 intramolecular and 28 intermolecular protein-protein crosslinks within the tetrameric complex (Tables S2 and S3). The crosslinking distances are all in the expected range of ≤30 Å and are in agreement with the arrangement of Nup214, CRM1, SPN1, and RanGTP in the crystal structure (Figure S5). Importantly, we also identified two crosslinking sites between Nup214 and SPN1 (Nup214 K1928–SPN1 K223) and CRM1 (Nup214 K2010–CRM1 K22), respectively. Both sites are consistent with the location of the FG motifs of Nup214 on the trimeric export complex (Table S3; Figure S5). The in-solution crosslinking data verify the interactions observed in the crystal structure, specifically the interactions of FG region 1 that could be influenced by the close proximity of the MBP tag and the interaction of F2 with a symmetry-related CRM1 molecule.

Functional Characterization of CRM1-Nup214 Interactions

Our structural analysis revealed a large number of contacts between CRM1 and the Nup214 fragment, most of which are based on hydrophobic interactions. Thus, we analyzed the functional consequences of changing interacting residues, both in Nup214 fragments as well as in CRM1. Nup214 mutants were created with exchanges of phenylalanines to serines. A Nup214 mutant with all the phenylalanines that bound to the C-terminal arch of CRM1 in the crystal structure (F1–F6) mutated to serines was termed "Nup214-X1". In the Nup214-X2 mutant, phenylalanines that bound to the N-terminal arch of CRM1 (F7 to F8) were mutated to serines. The Nup214-X3 mutant was a combination of X1 and X2 (Figure 4A).

First, we compared the ability of Nup214$_{1,916–2,033}$ mutants to promote binding of CRM1 to immobilized HIV-1 Rev (compare Figure 1B). Nup214-X1 and -X2 were still able to stabilize the CRM1-RanGTP-HIV-1 Rev complex, although to a lower extent than the wild-type version (Figure 4B). For Nup214-X3, only very little CRM1 binding to HIV-1 Rev was observed, indicating a strongly reduced affinity of the Nup214 fragment for the export receptor. For a quantitative analysis, the ability of the mutant Nup214 fragments to interact with wild-type CRM1 was analyzed by RanGAP assays. The wild-type Nup214 fragment

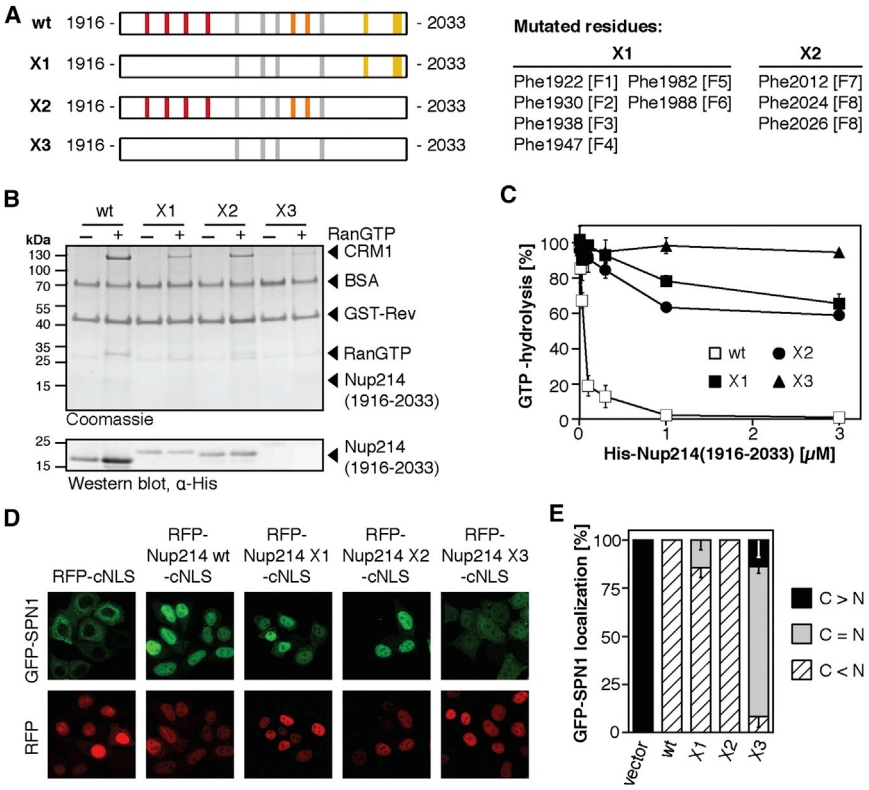

Figure 4. Phenylalanines in Nup214 Are Important for CRM1 Binding

(A) Schematic representation of recombinant Nup214 fragments. FG motifs are marked in gray or colored as in Figures 2 and 3 if visible in the crystal structure. F1–8 indicate the phenylalanines as specified in Figure 3.

(B) 100 pmol GST-HIV-1 Rev was immobilized on glutathione beads and incubated with CRM1 and the respective His-Nup214$_{1,916–2,033}$ fragment in the absence or presence of 750 nM RanGTP$_{Q69L}$. Bound proteins were analyzed by SDS-PAGE, followed by Coomassie staining or western blotting.

(C) RanGAP-assays were performed with increasing concentrations of wild-type His-Nup214$_{1,916–2,033}$ or mutants X1, X2, or X3, as indicated. All reactions contained 500 nM CRM1. Error bars indicate the SD from the mean of three independent experiments.

(D and E) HeLa cells were co-transfected with plasmids coding for GFP-SPN1 and RFP-cNLS or Nup214$_{1,859–2,090}$ fragments fused to RFP-cNLS. Cells were analyzed by fluorescence microscopy (D; bar, 20 μm) and the localization of GFP-SPN1 in 100 cells was categorized as predominantly cytoplasmic (C > N), equally distributed (C = N), and predominantly nuclear (C < N). (E) The mean and SD of at least three independent experiments are plotted.

led to a strong reduction of RanGAP-induced GTP hydrolysis, indicating the formation of a RanGAP-resistant CRM1-RanGTP-Nup214 complex (Figure 4C). Mutants X1, X2, and X3, by contrast, had hardly any effect in this assay. Of note, mutation of only three residues within FG region 3 in the Nup214-X2 fragment almost completely abolished GTPase protection. These results indicate that, in the context of the Nup214$_{1,916–2,033}$ fragment, the identified phenylalanines play an important role in CRM1 binding.

Next, we used a cell-based assay to test whether longer Nup214 fragments (aas 1,859–2,090), containing nine additional FG repeats, with the same mutations (X1, X2, and X3) affected CRM1 binding. In this system, the localization of GFP-SPN1, which normally resides in the cytoplasm due to CRM1-mediated nuclear export, is analyzed in cells that express Nup214 fragments fused to RFP-cNLS. In the nucleus, they can interact with CRM1 and thereby inhibit nuclear export. The wild-type Nup214 fragment led to a clear shift of GFP-SPN1 from the cytoplasm to the nucleus, indicating efficient interaction with CRM1 (Figures 4D and 4E). Nup214 mutants X1 and X2 had almost the same effect as the wild-type fragment, demonstrating that the exchange of phenylalanines that either bind to the C-terminal (X1) or the N-terminal (X2) arch of CRM1 did not prevent the Nup214-CRM1 interaction. Strikingly, when the two sets of mutations were combined in the X3 mutant, the resulting Nup214 fragment was far less efficient in inhibiting SPN1 export, suggesting reduced CRM1 binding. These results confirm the importance of the identified FG motifs in Nup214 for CRM1 interaction.

Our results also suggest that mutations within individual FG-binding pockets of CRM1, which are expected to affect only one out of many Nup214 contacts, might not have strong effects on nucleoporin interactions in general. Nevertheless, we generated a set of CRM1 mutants with amino acid changes in the identified FG-binding pockets. Several CRM1 mutants containing only a single mutation were completely insoluble under conditions that yielded milligram quantities of the wild-type protein. For mutants that could be purified in sufficient quantities, we first performed binding assays using phenyl-Sepharose as an interaction matrix. Phenyl-Sepharose has previously been used to enrich transport receptors from cytosol (Ribbeck and Görlich, 2002) and also to monitor differences of CRM1 mutants (Koyama et al., 2014). No differences in binding to phenyl-Sepharose were observed for our tested CRM1 mutants in the absence or presence of RanGTP or NES peptide (data not shown). We therefore decided to more carefully analyze the CRM1-Nup214 interactions. Due to the allosteric character of CRM1, the mutation of an individual residue in a Nup214-binding site could affect the arrangements of the HEAT repeats, thereby influencing distant binding sites of Ran and cargo. To faithfully characterize CRM1 mutants with respect to nucleoporin binding, the mutations should not affect binding of either RanGTP or the export cargo. We used RanGAP assays to assess these parameters. Two of the CRM1 mutants, CRM1 (S928K) and CRM1 (A156F), showed clear differences in RanGTP/cargo binding compared to wild-type CRM1 (Figure 5A), even though the mutated residues are not necessarily in close proximity to the RanGTP- or cargo-binding regions. Four of the tested CRM1 mutants showed

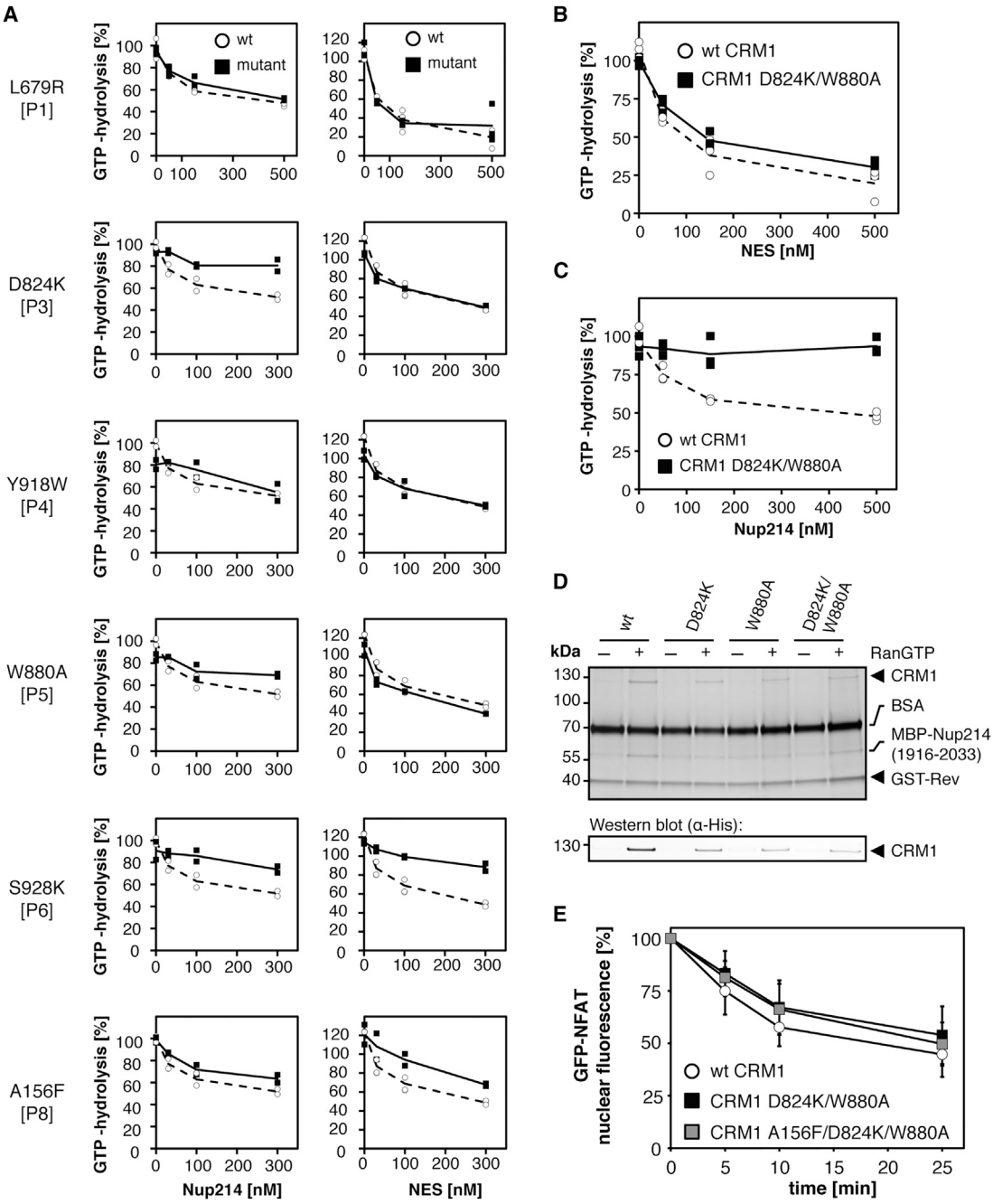

Figure 5. CRM1 Mutations in FG-Binding Patches Affect Nucleoporin and NES Binding

(A–C) RanGAP assays were performed with 300 nM of wild-type CRM1 or CRM1 single mutants (A) or the CRM1 (D824K/W880A) mutant (B and C), respectively, in the presence of increasing concentrations of MBP-Nup214$_{1,916–2,033}$ (A, left panel, and C) or NES peptide (A, right panel, and B). The individual values and averages of two independent experiments (mutants, solid lines; wild-type, dashed lines) are shown.

(D) 50 pmol GST-Rev was immobilized on glutathione beads and incubated with MBP-Nup214$_{1,916–2,033}$ and wild-type CRM1 (wt) or CRM1 mutants in the absence or presence of RanGTP. Bound proteins were analyzed by SDS-PAGE, followed by Coomassie staining and western blotting.

(E) Permeabilized GFP-NFAT cells were incubated with 100 nM of wild-type CRM1, CRM1 (D824K/W880A), or CRM1 (A156F/D824K/W880A). After the export reaction, residual nuclear fluorescence was analyzed by flow cytometry. Values were normalized to fluorescence intensities at 0 min.

See also Figure S6.

NES-titration profiles very similar to that of the wild-type protein, namely CRM1 (L679R), CRM1 (D824K), CRM1 (Y918W), and CRM1 (W880A), with mutations in P1, P3, P4, and P5, respectively (Figure 5A). Despite these shortcomings, we tested all of the CRM1 mutants in RanGAP assays with the $Nup214_{1,916–2,033}$ fragment that was used for crystallization. Remarkably, almost all of the CRM1 mutants showed reduced interaction with the Nup214 fragment. In particular, two CRM1 mutants (D824K and W880A) that were not affected with respect to RanGTP/NES interaction were less efficient than wild-type CRM1 in inhibiting RanGAP-induced GTP hydrolysis in the presence of increasing concentrations of the Nup214 fragment (Figure 5A).

To analyze the effect of a CRM1 variant containing mutations in multiple FG pockets, we combined the two mutations creating the double mutant CRM1 (D824K/W880A). Similar to the individual mutations, RanGTP/NES binding was not affected in this double mutant (Figure 5B). Strikingly, an interaction with the $Nup214_{1,916–2,033}$ fragment was hardly detected for this CRM1 mutant in RanGAP assays (Figure 5C). To corroborate these findings, we analyzed the Nup214-CRM1 interaction in direct binding assays. We immobilized the CRM1-cargo HIV-1 Rev (Figure 5D) and tested the ability of the $Nup214_{1,916–2,033}$ fragment to promote binding of mutant CRM1 to HIV-1 Rev. Less of the CRM1 single mutants D824K and W880A or of the double mutant CRM1 (D824K/W880A) was recovered in this binding assay in comparison to wild-type CRM1, confirming a reduced affinity of the export receptor for the Nup214 fragment. The defect of CRM1 mutants in Nup214 binding got more prominent when a shorter Nup214 fragment was used (Figure S6A). Binding of CRM1 to phenyl-Sepharose, by contrast, was not affected by either single or double mutations (Figure S6B), demonstrating that this approach is not suitable for the detection of subtle changes in binding affinities.

Together, these results show that amino acid residue exchanges within most of the identified FG-binding pockets in CRM1 affect nucleoporin binding. As expected for a protein with multiple binding sites, the effects of mutating individual sites were rather mild.

We next asked the question of whether the double mutant CRM1 (D824K/W880A) or the triple mutant CRM1 (A156F/D824K/W880A) with mutated FG-binding pockets on the C- and the N-terminal arch would support nuclear export to the same extent as the wild-type protein. In our well-established in vitro transport assay, wild-type and mutant CRM1 supported nuclear export of GFP-NFAT to very similar extents (Figure 5E). This result suggests that amino acid changes in CRM1 that clearly affect binding to isolated nucleoporins or regions of nucleoporins may not result in drastic changes of the overall avidity of the export receptor to the NPC and, hence, do not affect the kinetics of nuclear export.

Interaction of CRM1 with Other Nucleoporins and Nucleoporin-like Proteins

To determine whether the amino acids forming the individual FG-binding pockets on CRM1 are conserved, we performed a comprehensive alignment with 16 CRM1 orthologs comprising sequences from vertebrates, fungi, insects, and protozoa (Figure 6A). Besides known regions with high sequence conservation, namely the NES-binding cleft and surface patches involved in Ran binding (Monecke et al., 2014), P7 and P8 within FG-binding patch 3 are highly conserved among those very distantly related species (Figure 6D). FG-binding patch 2, comprising P5 and P6, is equally conserved (Figure 6C), whereas P1, P3, and P4 of FG-binding patch 1 show less conservation (Figure 6B).

Based on this conservation, we speculated that at least some of the identified FG-binding pockets on CRM1 are also involved in binding of other nucleoporins. Thus, we performed competition experiments to confirm that Nup214 and Nup62, another bona fide nucleoporin, bind to similar regions on CRM1. We used a semiquantitative assay to monitor RanGTP- and NES-peptide-dependent binding of fluorescently labeled CRM1 to an immobilized Nup214 fragment (Figure 6E). Nup62 and Nup214 competed for binding to CRM1, suggesting that they contact similar binding sites. Notably, much higher concentrations of Nup62 were required to reduce binding of CRM1 to immobilized Nup214 fragments than of soluble Nup214 in a reciprocal experiment, where Nup62 had been immobilized on beads (Figure 6F). This probably reflects the very high affinity of Nup214 for the CRM1 export complex (Hutten and Kehlenbach, 2006).

Similar results were obtained when we used RanBP3, an FG repeat containing nucleoporin-like protein in such a competition pull-down assay. $Nup214_{1,930–2,021}$ was immobilized and incubated with CRM1, SPN1, RanGTP, and increasing amounts of RanBP3. The addition of RanBP3 to the reaction strongly reduced the interaction of CRM1 with the nucleoporin fragment, suggesting that binding of the export receptor to Nup214 and RanBP3 is mutually exclusive (Figure 6G). This observation is perfectly in line with the structure of the yeast CRM1-RanGTP-RanBP3 complex (Koyama et al., 2014). Here, two FG repeat regions of RanBP3 bind to H17–20 as well as H2–4 of CRM1 overlapping with FG-binding patches 2 and 3 in our Nup214 export complex (Figure 7). Although the FG-binding patches on CRM1 largely overlap, the interaction details differ. For example, the second FG repeat region of RanBP3 binds to the N-terminal H2–4 of CRM1 and contains three FG motifs, which are bound by three distinct FG-binding pockets on CRM1 (Figure 7C). In contrast, the region of Nup214 binding to the same HEAT repeats harbors only two such FG motifs. In addition to two FG-binding patches on CRM1 in the CRM1-RanGTP-RanBP3 complex, a third major binding patch in the central region of CRM1 (H14–19) was observed for Nup214.

Together, these results indicate that highly conserved residues on CRM1 mediate the interaction with proteins of the NPC or with accessory factors like RanBP3 that contain appropriate binding motifs.

DISCUSSION

Unraveling the molecular details of nucleoporin-karyopherin interactions, which have to be strong enough to promote transport but sufficiently weak to avoid stalling of transport complexes within the pore, is key to our understanding of the mechanisms of nucleocytoplasmic transport. The interactions of CRM1 and Nup214 can serve as a paradigm for karyopherin-nucleoporin

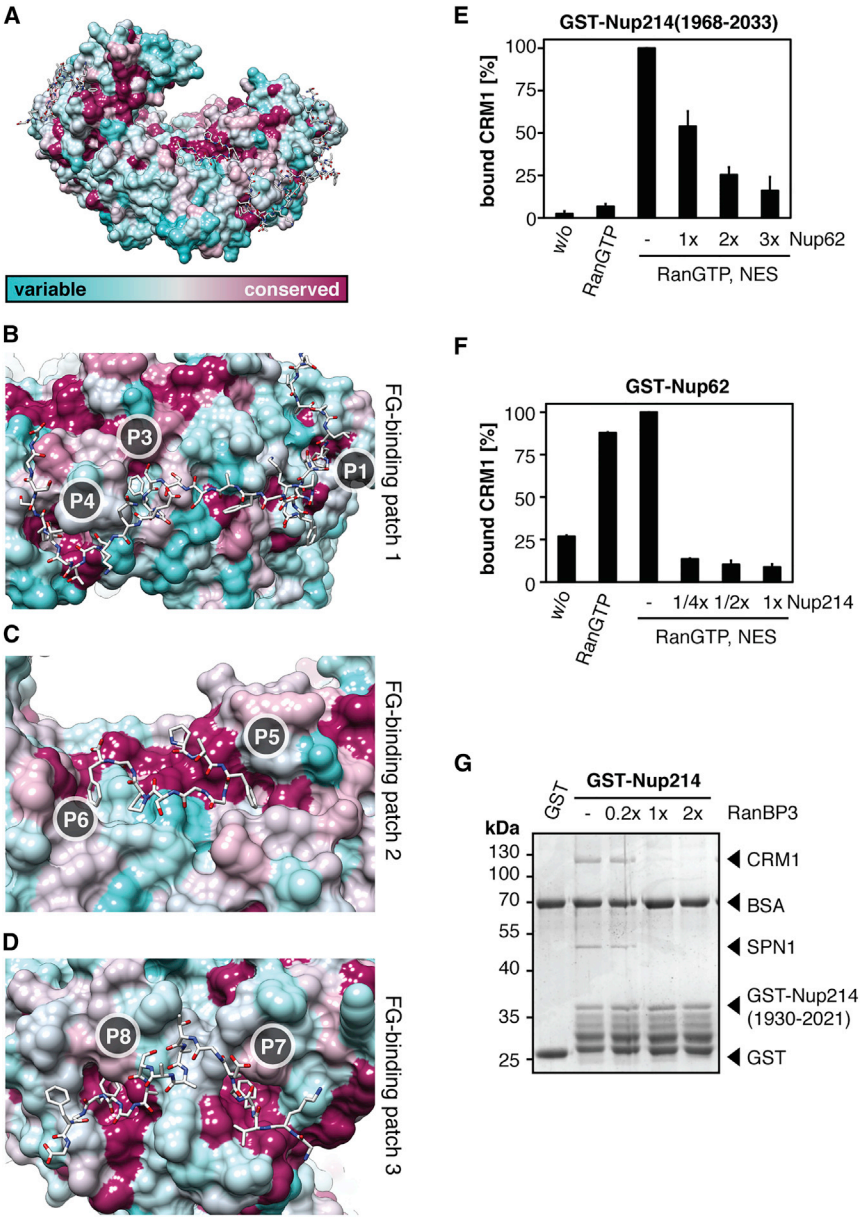

Figure 6. CRM1 Conservation and Nup214 Competition by RanBP3 and Nup62 FG Repeats

Sequence conservation of CRM1 FG-pockets in the structural context of the Nup214 export complex.

(A–D) Overall view (A) and detailed views (B–D) of FG-binding regions 1–3 of CRM1 bound to FG motifs of Nup214. CRM1 is depicted as surface and colored according to sequence conservation from invariant or strictly conserved (dark red) to variable (cyan). Nup214 residues are depicted as sticks (carbon in white, nitrogen in blue, and oxygen in red). Note that the binding pockets for FG motifs 7 and 8 as well as FG-binding region 2 are strongly conserved among 16 aligned CRM1 orthologs, whereas FG-binding region 1 is less conserved.

(E and F) 50 pmol GST-Nup214$_{1,968–2,033}$ (E) or 50 pmol GST-Nup62 (F) were immobilized on beads and incubated with Cy3-labeled CRM1, alone or in the presence of 9 μM RanGTP$_{Q69L}$ and 50 μM NES peptide and increasing amounts of Nup62 (0/50/100/150 pmol) or His-Nup214$_{1,916–2,033}$ (0/12.5/25/50 pmol), respectively. Bound Cy3-CRM1 was analyzed by flow cytometry.

(G) 250 pmol GST or GST-Nup214$_{1,930–2,021}$ was immobilized on glutathione beads and incubated with purified CRM1-RanGTP$_{Q69L}$-SPN1 export complex and increasing amounts of RanBP3 (50/250/500 pmol). Bound proteins were analyzed by SDS-PAGE, followed by Coomassie staining.

interactions in general. In this study, we solved the structure of a CRM1 export complex bound to a 117-amino-acid fragment of Nup214 at multiple FG motifs. We identified three FG regions in the Nup214 fragment containing a total of seven characteristic FG motifs and a similar FS motif (F1–F8). The location of FG-binding patches 2 and 3 on the N-terminal and C-terminal arches of CRM1, respectively, is consistent with a recently reported crystal structure (PDB: 3WYF) of yeast CRM1 (Xpo1p) bound to RanGTP (Gsp1p) and RanBP3 (Yrb2p; Figure 7). RanBP3, however, contains only five FG motifs in two FG regions, and binding to CRM1 occurs mainly via its Ran-binding domain. Almost all of the phenylalanine residues in the Nup214 fragment bind to corresponding hydrophobic pockets in CRM1 (P1–P8). In order to insert these large side chains between two HEAT helices and form intricate interactions with hydrophobic residues between them, a kink in the main chain of the nucleoporin is required. To enable such a large (~180°) bending of the peptide chain, the phenylalanine is followed by an adjacent glycine residue forming a sharp β turn, resulting in hydrogen bonding between the main chain carbonyl of residue n and the main chain amine of residue n + 3. Similar arrangements were previously described for a fragment of importin β binding to an FxFG motif (Bayliss et al., 2000) and for the CRM1-RanBP3 interaction (Koyama et al., 2014).

Strikingly, FG-binding pockets from the N- and C-terminal region of CRM1 bind to FG motifs on Nup214 that are separated by a rather short stretch of amino acids. This is possible because, in the context of an export complex, the CRM1 termini are in close proximity, allowing simultaneous binding of the extended Nup214 fragment to the FG-binding pockets in CRM1. CRM1 can also be held together in a closed conformation by the Nup214 fragment in the presence of RanGTP but in the absence of an export substrate (Figure 1A). Thus, Nup214 functions as a molecular clamp, leading to stabilization of the export complex. This function, which requires binding of the nucleoporin to multiple sites of the export receptor, becomes obvious when we

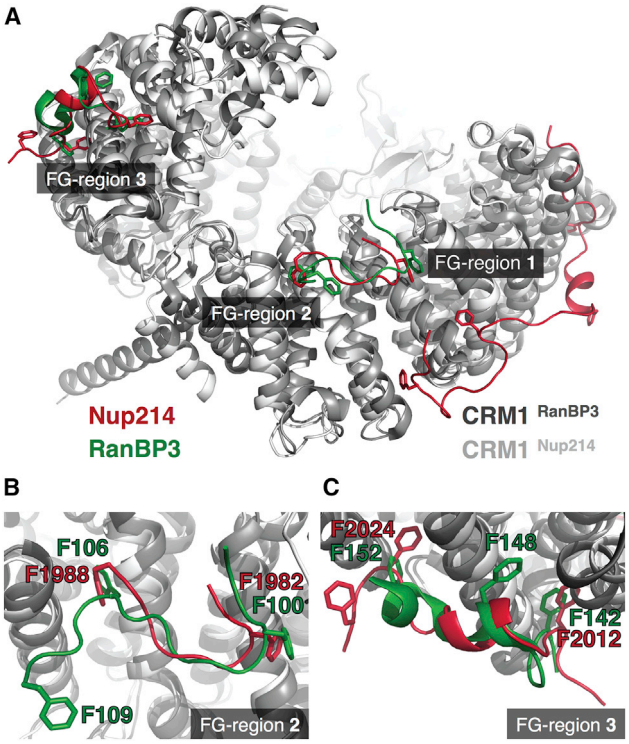

Figure 7. Comparison of the Crystal Structures of CRM1 in Complex with FG Motifs of Nup214 and RanBP3

(A) Overall superposition of CRM1 (light and dark gray) and FG repeats of Nup214 (red) and RanBP3 (PDB: 3WYF; green). Note that the two FG regions of RanBP3 overlap with FG regions 2 and 3 of Nup214. FG region 1 of Nup214 has no counterpart in RanBP3.

(B and C) Detailed views on the superposition at FG-binding patches 2 and 3 of CRM1. Although the FG-binding patches on CRM1 are identical for Nup214 and RanBP3, the interactions and details of binding (e.g., depth of the Phe-pocket and course of the peptide chain) differ in both structures.

compare the effects of mutations within the Nup214 sequence in different assays. The Nup214-X2 mutant, for example, where three phenylalanine residues are changed to serines, still bound the CRM1 export complex in pull-down experiments, similar to the wild-type protein (Figure 4B). However, in assays where we monitored the ability of the nucleoporin fragment to protect CRM1-bound RanGTP from RanGAP-induced GTP hydrolysis, the Nup214-X2 mutant, which according to the structure should only bind to the C-terminal arch of CRM1, showed only a very weak effect compared to the wild-type fragment (Figure 4C). Similar observations were made for the Nup214-X1 mutant, which should only bind to the N-terminal region of CRM1. Thus, simple binding is not sufficient to protect CRM1 from GTP hydrolysis. This effect rather requires the clamp function of Nup214 with simultaneous binding to both ends of the export receptor. Cooperative binding of all four components of the CRM1-RanGTP-cargo-Nup214 complex is further enhanced by subtle changes in FG pockets of CRM1 upon formation of the trimeric export complexes that initially lack the nucleoporin. For export substrate-containing complexes, the stabilizing effect of FG nucleoporins distinct from Nup214 should prevent premature loss of the cargo during transit.

The NES-binding site in CRM1 is the most-conserved part of the export receptor (Monecke et al., 2014). Our analysis reveals that regions containing several of the FG-binding pockets in CRM1 are also conserved among species (Figure 6A). Interestingly, mutations in these regions affected binding of RanGTP and/or an NES substrate underlining the allosteric nature of CRM1 and suggesting that the overall CRM1 structure is extremely sensitive with respect to amino acid changes. Thus, for all functional assays in intact cells or in permeabilized systems, possible side effects of even single point mutations in transport receptors must be considered. In light of our observation that binding of CRM1 to Nup214 and other nucleoporins (Nup62) or nucleoporin-like proteins (RanBP3) is mutually exclusive, we conclude that the CRM1 sequence has been optimized during evolution to interact via similar mechanisms with a multitude of FG-containing proteins, as they are encountered during passage of the NPC—without compromising the ability of CRM1 to bind its primary partners, RanGTP and NES cargo. Interestingly, we observed that the FG pocket for $Phe1922^{Nup214}$ (P1) partially overlaps with the binding site for the C-terminal 12 residues of SPN1, representing its third CRM1-binding epitope in the ternary export complex structure (PDB: 3GJX; Figure S3). It has previously been reported that a truncated version of SPN1, lacking these C-terminal residues, binds CRM1 with a 60% lower affinity (Paraskeva et al., 1999). Due to the cooperative binding of SPN1 and Nup214 to CRM1, it is difficult to distinguish between the respective contributions of SPN1 and Nup214 to complex stability. However, the electron density for Nup214 in this region was significantly weaker when crystals with full-length SPN1 and the same Nup214 fragment were used for structure determination (data not shown). This could indicate a rather dynamic and/or mutual exclusive binding of Nup214 and the SPN1 C terminus. Thus, the overlapping binding sites might function in the release of the export complex, as binding of Nup214 to that site probably lowers the affinity of SPN1 to CRM1.

Other karyopherins besides CRM1 must bind to FG-Nups in a similar fashion. However, at an atomic resolution, only the interaction of importin β with isolated FG motifs has been analyzed (Bayliss et al., 2000, 2002; Liu and Stewart, 2005). Despite similarities in the FG-binding pockets of CRM1 and other transport receptors, the export receptor has a particularly high affinity for Nup214 (Figure 1A).

From the nucleoporin's point of view, interactions with transport receptors have to fulfill two opposing functions: first, binding must be strong enough to discriminate between bona fide transport complexes (or empty transport receptors) and inert proteins, whose translocation through the pore should be obstructed. On the other hand, interactions at individual binding sites must be weak to allow release of transport complexes and their translocation within the time frame of milliseconds. Our results clearly show that there are many interaction sites between CRM1 and nucleoporins. Full-length Nup214 contains a total of 44 FG motifs, 32 of which are not present in the fragment that was used for crystallization. Hence, additional contacts between CRM1 and several of these FG sites

are likely and may further contribute to a high-avidity interaction. Apart from a study that showed three interaction sites between a nucleoporin fragment and Kap95p (Liu and Stewart, 2005), multiple binding sites on transport receptors for FG motifs have so far only been simulated (Isgro and Schulten, 2005). Importantly, each of the multiple FG-binding pockets, which contact FG motifs on a rather linear, initially unstructured stretch of amino acids of FG-Nups, is expected to contribute only weakly to the overall avidity of the complex. Our structure shows that intervening Nup sequences are hardly attached to the transport receptor and will therefore be flexible upon loosening a single FG contact. Rapid dissociation of single sites, followed by rebinding of the transport receptor to a close-by FG motif (possibly of another nucleoporin) should therefore be feasible. Such association/dissociation cycles should allow the transport complex to overcome the permeability barrier of the NPC. For CRM1 export complexes, GTP hydrolysis on Ran as promoted by cytoplasmic RanGAP ultimately leads to dissociation of the CRM1 export complex from a terminal binding site, e.g., at the cytoplasmic nucleoporin Nup214 (Kehlenbach et al., 1999).

With respect to the kinetics of nuclear export, we cannot expect drastic changes upon manipulation of individual FG pockets within the CRM1 molecule, because the overall avidity of the transport receptor for nucleoporins in general will hardly be affected. Indeed, our double mutant CRM1 (D824K/W880A), which showed reduced binding to Nup214 fragments (Figures 5C and 5D), and even the triple mutant CRM1 (A156F/D824K/W880A) were as efficient in promoting nuclear export of GFP-NFAT as the wild-type protein (Figure 5E). The functional assay integrates possible interactions of CRM1 with full-length Nup214 and with all other FG nucleoporins, which may contribute to efficient passage of export complexes through the nuclear pore.

The mode of interaction of nuclear transport receptors with nucleoporins is of paramount importance for the mechanisms of nucleocytoplasmic transport. With CRM1 as an example, we are beginning to understand the molecular details of transport complexes passing through the permeability barrier of the NPC, a process that involves binding to local FG regions, but also rapid dissociation from such sites. Based on the principles described above, movement of transport complexes within the pore becomes feasible, without bringing translocation to a standstill due to slow off rates.

EXPERIMENTAL PROCEDURES

Protein Expression and Purification

Proteins were expressed in *E. coli* and purified as described in the Supplemental Experimental Procedures.

Preparation, Crystallization, and Structure Determination of the Nup214 Export Complex

The CRM1-SPN1-RanGTP-$_{MBP}$Nup214 complex was purified using gel filtration chromatography and crystallized by vapor diffusion in PEG8000-containing conditions. Orthorhombic crystals were subjected to successive PEG-mediated crystal dehydration, treated using a crystal humidifier (HC1c), flash-cooled in liquid nitrogen, and measured. The crystal structure was solved and refined as described in Supplemental Experimental Procedures. See also Figure S1.

Pull-Downs

GST fusion proteins were immobilized on glutathione Sepharose (GE Healthcare) equilibrated in pull-down buffer (50 mM Tris [pH 7.4], 200 mM NaCl, 1 mM $MgCl_2$, 5% glycerol, 1 mM DTT, and 20 mg/ml BSA). The beads were incubated with proteins of interest in a total volume of 400 μl for 1 hr at 4°C and washed three times with 500 μl pull-down buffer lacking BSA. Bound proteins were eluted in 2× SDS sample buffer and analyzed by SDS-PAGE followed by Coomassie staining or western blotting.

Flow-Cytometry-Based Binding Assay

CRM1 was labeled with Cy3 (Mono Reactive Dye Pack; GE Healthcare). 50 pmol GST fusion protein was immobilized on 2.5 μl glutathione Sepharose (GE Healthcare) equilibrated in transport buffer (20 mM HEPES [pH 7.3], 110 mM KOAc, 2 mM $Mg(OAc)_2$, 1 mM EGTA, and 1 mM DTT) supplemented with 10 mg/ml BSA. The beads were washed and incubated with 7.3 pmol CRM1-Cy3, other proteins of interest, and 4× assay mix (500 mM NaCl, 40 mg/ml BSA, 1 mM DTT, and 2% 1,6-hexanediole) in a total volume of 20 μl transport buffer containing 10 mg/ml BSA for 1 hr at 4°C. The beads were washed with transport buffer and bound CRM1-Cy3 was analyzed by flow cytometry using a FACSCanto II (BD Biosciences) and FACS Diva 6.1.1 software. The median fluorescence of 10,000 beads was measured (585/42 bandwidth and 556LP filter).

RanGAP Assays

RanGAP assays were performed as described previously (Askjaer et al., 1999; Kehlenbach et al., 1999). Briefly, CRM1 wild-type or mutants were incubated with Ran loaded with ^{32}P-γ-GTP and increasing concentrations of Nup214 fragments or full-length SPN1 or the NES peptide of minute virus of mice (CVDEMTKKFGTLTIHDTEK) as export cargo. GTP hydrolysis was initiated by the addition of 10 nM RanGAP and analyzed by determining free radioactive phosphate. Results were normalized to a reaction without RanGAP and plotted as percent of maximal GTP hydrolysis.

Transfection of Mammalian Cells

HeLa p4 cells (Charneau et al., 1994) were grown in 24-well plates. Plasmids coding for GFP-SPN1 and RFP-Nup214-cNLS fragments were co-transfected with the calcium phosphate method (Ausubel et al., 1994). The effect of Nup214 or CRM mutants on nuclear export was analyzed by quantifying the distribution of GFP-SPN1.

In Vitro Export Assays

Transport assays were adapted from Kehlenbach et al. (1998). Permeabilized GFP-NFAT cells were pre-treated in transport buffer with an ATP-regenerating system (1 mM ATP, 4 mM creatine phosphate, and 10 U/ml creatine phosphokinase) and 100 nM LMB in a 30°C water bath for 15 min to remove soluble transport factors and block endogenous CRM1. Export reactions contained 100,000 pre-incubated cells, 2 μM Ran, an ATP-regenerating system, 1 μM oligonucleotides (5′AGAGGAAAATTTGTTTCATA and 5′ TATGAAACAAAT TTTCCTCT), and wild-type CRM1 or CRM1 mutant and were incubated at 30°C. Reactions were stopped with ice-cold transport buffer, and the efficiency of export was analyzed by measuring the residual median fluorescence of GFP-NFAT in 5,000 cells using a FACSCanto II flow cytometer (BD Biosciences).

ACCESSION NUMBERS

The accession number for the atomic coordinates and structure factors of the CRM1-RanGTP-SPN1-$_{MBP}$Nup214 complex reported in this paper is PDB: 5DIS.

SUPPLEMENTAL INFORMATION

Supplemental Information includes Supplemental Experimental Procedures, six figures, and four tables and can be found with this article online at http://dx.doi.org/10.1016/j.celrep.2015.09.042.

AUTHOR CONTRIBUTIONS

S.A.P., T.M., A.D., R.H.K., and R.F. conceived the project, analyzed results, and wrote the manuscript. S.A.P. and T.M. purified proteins, and S.A.P. performed biochemical and cell biological analyses. S.A.P. and T.M. set up crystallization trials, and T.M. solved the structure. C.S. generated molecular biology reagents. R.H. and H.U. performed the MS analysis and interpreted the results.

ACKNOWLEDGMENTS

We thank Uwe Plessmann and Monika Raabe for excellent technical assistance in LC-MSMS and Carolin Thüne for valuable assistance in protein purification. We are very grateful to Piotr Neumann for his strong crystallographic support as well as Andreas Schmitt for help with figures. We also wish to thank Imke Baade for purifying importin 13, Dirk Görlich for reagents, and Cara Jamieson for very helpful comments on the manuscript. This work was supported by the DFG, Sonderforschungsbereich 860 (to H.U., R.F., and R.H.K.). We also acknowledge support by the Open Access Publication Funds of the Göttingen University.

Received: June 12, 2015
Revised: August 11, 2015
Accepted: September 14, 2015
Published: October 15, 2015

REFERENCES

Askjaer, P., Bachi, A., Wilm, M., Bischoff, F.R., Weeks, D.L., Ogniewski, V., Ohno, M., Niehrs, C., Kjems, J., Mattaj, I.W., and Fornerod, M. (1999). RanGTP-regulated interactions of CRM1 with nucleoporins and a shuttling DEAD-box helicase. Mol. Cell. Biol. *19*, 6276–6285.

Ausubel, F.M., Brent, R., Kingston, R.E., Moore, D.D., Seidman, J.G., Smith, J.A., and Struhl, K. (1994). Current Protocols in Molecular Biology (New York: Greene Publishing Associates and Wiley-Interscience).

Bayliss, R., Littlewood, T., and Stewart, M. (2000). Structural basis for the interaction between FxFG nucleoporin repeats and importin-beta in nuclear trafficking. Cell *102*, 99–108.

Bayliss, R., Littlewood, T., Strawn, L.A., Wente, S.R., and Stewart, M. (2002). GLFG and FxFG nucleoporins bind to overlapping sites on importin-beta. J. Biol. Chem. *277*, 50597–50606.

Bernad, R., Engelsma, D., Sanderson, H., Pickersgill, H., and Fornerod, M. (2006). Nup214-Nup88 nucleoporin subcomplex is required for CRM1-mediated 60 S preribosomal nuclear export. J. Biol. Chem. *281*, 19378–19386.

Charneau, P., Mirambeau, G., Roux, P., Paulous, S., Buc, H., and Clavel, F. (1994). HIV-1 reverse transcription. A termination step at the center of the genome. J. Mol. Biol. *241*, 651–662.

Chi, N.C., Adam, E.J.H., and Adam, S.A. (1997). Different binding domains for Ran-GTP and Ran-GDP/RanBP1 on nuclear import factor p97. J. Biol. Chem. *272*, 6818–6822.

Cook, A., Bono, F., Jinek, M., and Conti, E. (2007). Structural biology of nucleocytoplasmic transport. Annu. Rev. Biochem. *76*, 647–671.

Denning, D.P., Patel, S.S., Uversky, V., Fink, A.L., and Rexach, M. (2003). Disorder in the nuclear pore complex: the FG repeat regions of nucleoporins are natively unfolded. Proc. Natl. Acad. Sci. USA *100*, 2450–2455.

Dong, X., Biswas, A., and Chook, Y.M. (2009a). Structural basis for assembly and disassembly of the CRM1 nuclear export complex. Nat. Struct. Mol. Biol. *16*, 558–560.

Dong, X., Biswas, A., Süel, K.E., Jackson, L.K., Martinez, R., Gu, H., and Chook, Y.M. (2009b). Structural basis for leucine-rich nuclear export signal recognition by CRM1. Nature *458*, 1136–1141.

Englmeier, L., Fornerod, M., Bischoff, F.R., Petosa, C., Mattaj, I.W., and Kutay, U. (2001). RanBP3 influences interactions between CRM1 and its nuclear protein export substrates. EMBO Rep. *2*, 926–932.

Floer, M., and Blobel, G. (1996). The nuclear transport factor karyopherin beta binds stoichiometrically to Ran-GTP and inhibits the Ran GTPase activating protein. J. Biol. Chem. *271*, 5313–5316.

Fornerod, M., Boer, J., van Baal, S., Morreau, H., and Grosveld, G. (1996). Interaction of cellular proteins with the leukemia specific fusion proteins DEK-CAN and SET-CAN and their normal counterpart, the nucleoporin CAN. Oncogene *13*, 1801–1808.

Fornerod, M., Ohno, M., Yoshida, M., and Mattaj, I.W. (1997a). CRM1 is an export receptor for leucine-rich nuclear export signals. Cell *90*, 1051–1060.

Fornerod, M., van Deursen, J., van Baal, S., Reynolds, A., Davis, D., Murti, K.G., Fransen, J., and Grosveld, G. (1997b). The human homologue of yeast CRM1 is in a dynamic subcomplex with CAN/Nup214 and a novel nuclear pore component Nup88. EMBO J. *16*, 807–816.

Fukuda, M., Asano, S., Nakamura, T., Adachi, M., Yoshida, M., Yanagida, M., and Nishida, E. (1997). CRM1 is responsible for intracellular transport mediated by the nuclear export signal. Nature *390*, 308–311.

Görlich, D., Panté, N., Kutay, U., Aebi, U., and Bischoff, F.R. (1996). Identification of different roles for RanGDP and RanGTP in nuclear protein import. EMBO J. *15*, 5584–5594.

Grossman, E., Medalia, O., and Zwerger, M. (2012). Functional architecture of the nuclear pore complex. Annu. Rev. Biophys. *41*, 557–584.

Güttler, T., Madl, T., Neumann, P., Deichsel, D., Corsini, L., Monecke, T., Ficner, R., Sattler, M., and Görlich, D. (2010). NES consensus redefined by structures of PKI-type and Rev-type nuclear export signals bound to CRM1. Nat. Struct. Mol. Biol. *17*, 1367–1376.

Hülsmann, B.B., Labokha, A.A., and Görlich, D. (2012). The permeability of reconstituted nuclear pores provides direct evidence for the selective phase model. Cell *150*, 738–751.

Hutten, S., and Kehlenbach, R.H. (2006). Nup214 is required for CRM1-dependent nuclear protein export in vivo. Mol. Cell. Biol. *26*, 6772–6785.

Hutten, S., and Kehlenbach, R.H. (2007). CRM1-mediated nuclear export: to the pore and beyond. Trends Cell Biol. *17*, 193–201.

Iovine, M.K., Watkins, J.L., and Wente, S.R. (1995). The GLFG repetitive region of the nucleoporin Nup116p interacts with Kap95p, an essential yeast nuclear import factor. J. Cell Biol. *131*, 1699–1713.

Isgro, T.A., and Schulten, K. (2005). Binding dynamics of isolated nucleoporin repeat regions to importin-beta. Structure *13*, 1869–1879.

Kehlenbach, R.H., Dickmanns, A., and Gerace, L. (1998). Nucleocytoplasmic shuttling factors including Ran and CRM1 mediate nuclear export of NFAT In vitro. J. Cell Biol. *141*, 863–874.

Kehlenbach, R.H., Dickmanns, A., Kehlenbach, A., Guan, T., and Gerace, L. (1999). A role for RanBP1 in the release of CRM1 from the nuclear pore complex in a terminal step of nuclear export. J. Cell Biol. *145*, 645–657.

Kehlenbach, R.H., Assheuer, R., Kehlenbach, A., Becker, J., and Gerace, L. (2001). Stimulation of nuclear export and inhibition of nuclear import by a Ran mutant deficient in binding to Ran-binding protein 1. J. Biol. Chem. *276*, 14524–14531.

Kose, S., Imamoto, N., Tachibana, T., Shimamoto, T., and Yoneda, Y. (1997). Ran-unassisted nuclear migration of a 97-kD component of nuclear pore-targeting complex. J. Cell Biol. *139*, 841–849.

Koyama, M., Shirai, N., and Matsuura, Y. (2014). Structural insights into how Yrb2p accelerates the assembly of the Xpo1p nuclear export complex. Cell Rep. *9*, 983–995.

Kutay, U., Izaurralde, E., Bischoff, F.R., Mattaj, I.W., and Görlich, D. (1997). Dominant-negative mutants of importin-beta block multiple pathways of import and export through the nuclear pore complex. EMBO J. *16*, 1153–1163.

Lindsay, M.E., Holaska, J.M., Welch, K., Paschal, B.M., and Macara, I.G. (2001). Ran-binding protein 3 is a cofactor for Crm1-mediated nuclear protein export. J. Cell Biol. *153*, 1391–1402.

Liu, S.M., and Stewart, M. (2005). Structural basis for the high-affinity binding of nucleoporin Nup1p to the Saccharomyces cerevisiae importin-beta homologue, Kap95p. J. Mol. Biol. *349*, 515–525.

Monecke, T., Güttler, T., Neumann, P., Dickmanns, A., Görlich, D., and Ficner, R. (2009). Crystal structure of the nuclear export receptor CRM1 in complex with Snurportin1 and RanGTP. Science *324*, 1087–1091.

Monecke, T., Haselbach, D., Voß, B., Russek, A., Neumann, P., Thomson, E., Hurt, E., Zachariae, U., Stark, H., Grubmüller, H., et al. (2013). Structural basis for cooperativity of CRM1 export complex formation. Proc. Natl. Acad. Sci. USA *110*, 960–965.

Monecke, T., Dickmanns, A., and Ficner, R. (2014). Allosteric control of the exportin CRM1 unraveled by crystal structure analysis. FEBS J. *281*, 4179–4194.

Oka, M., Asally, M., Yasuda, Y., Ogawa, Y., Tachibana, T., and Yoneda, Y. (2010). The mobile FG nucleoporin Nup98 is a cofactor for Crm1-dependent protein export. Mol. Biol. Cell *21*, 1885–1896.

Ossareh-Nazari, B., Bachelerie, F., and Dargemont, C. (1997). Evidence for a role of CRM1 in signal-mediated nuclear protein export. Science *278*, 141–144.

Panté, N., Bastos, R., McMorrow, I., Burke, B., and Aebi, U. (1994). Interactions and three-dimensional localization of a group of nuclear pore complex proteins. J. Cell Biol. *126*, 603–617.

Paraskeva, E., Izaurralde, E., Bischoff, F.R., Huber, J., Kutay, U., Hartmann, E., Lührmann, R., and Görlich, D. (1999). CRM1-mediated recycling of snurportin 1 to the cytoplasm. J. Cell Biol. *145*, 255–264.

Rexach, M., and Blobel, G. (1995). Protein import into nuclei: association and dissociation reactions involving transport substrate, transport factors, and nucleoporins. Cell *83*, 683–692.

Ribbeck, K., and Görlich, D. (2002). The permeability barrier of nuclear pore complexes appears to operate via hydrophobic exclusion. EMBO J. *21*, 2664–2671.

Roloff, S., Spillner, C., and Kehlenbach, R.H. (2013). Several phenylalanine-glycine motives in the nucleoporin Nup214 are essential for binding of the nuclear export receptor CRM1. J. Biol. Chem. *288*, 3952–3963.

Stewart, M. (2007). Molecular mechanism of the nuclear protein import cycle. Nat. Rev. Mol. Cell Biol. *8*, 195–208.

Strawn, L.A., Shen, T., Shulga, N., Goldfarb, D.S., and Wente, S.R. (2004). Minimal nuclear pore complexes define FG repeat domains essential for transport. Nat. Cell Biol. *6*, 197–206.

Terry, L.J., and Wente, S.R. (2009). Flexible gates: dynamic topologies and functions for FG nucleoporins in nucleocytoplasmic transport. Eukaryot. Cell *8*, 1814–1827.

von Lindern, M., Poustka, A., Lerach, H., and Grosveld, G. (1990). The (6;9) chromosome translocation, associated with a specific subtype of acute non-lymphocytic leukemia, leads to aberrant transcription of a target gene on 9q34. Mol. Cell. Biol. *10*, 4016–4026.

Waldmann, I., Spillner, C., and Kehlenbach, R.H. (2012). The nucleoporin-like protein NLP1 (hCG1) promotes CRM1-dependent nuclear protein export. J. Cell Sci. *125*, 144–154.

Wente, S.R., and Rout, M.P. (2010). The nuclear pore complex and nuclear transport. Cold Spring Harb. Perspect. Biol. *2*, a000562.

Yokoyama, N., Hayashi, N., Seki, T., Panté, N., Ohba, T., Nishii, K., Kuma, K., Hayashida, T., Miyata, T., Aebi, U., et al. (1995). A giant nucleopore protein that binds Ran/TC4. Nature *376*, 184–188.

Cell Reports

Supplemental Information

Structural and Functional Characterization of CRM1-Nup214 Interactions Reveals Multiple FG-Binding Sites Involved in Nuclear Export

Sarah A. Port, Thomas Monecke, Achim Dickmanns, Christiane Spillner, Romina Hofele, Henning Urlaub, Ralf Ficner, and Ralph H. Kehlenbach

Figure S1

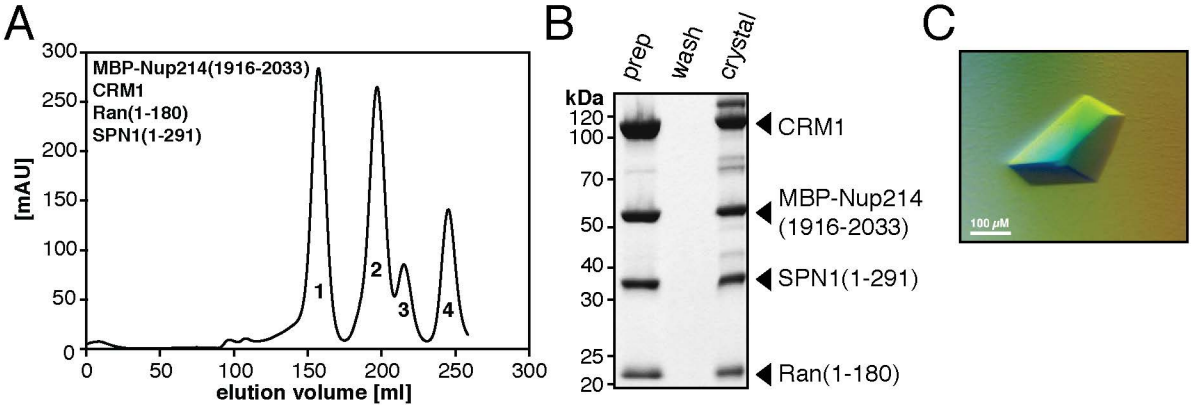
A
MBP-Nup214(1916-2033)
CRM1
Ran(1-180)
SPN1(1-291)
[mAU]
elution volume [ml]
1
2
3
4
B
prep
wash
crystal
kDa
CRM1
MBP-Nup214
(1916-2033)
SPN1(1-291)
Ran(1-180)
C
100 µM

Figure S2

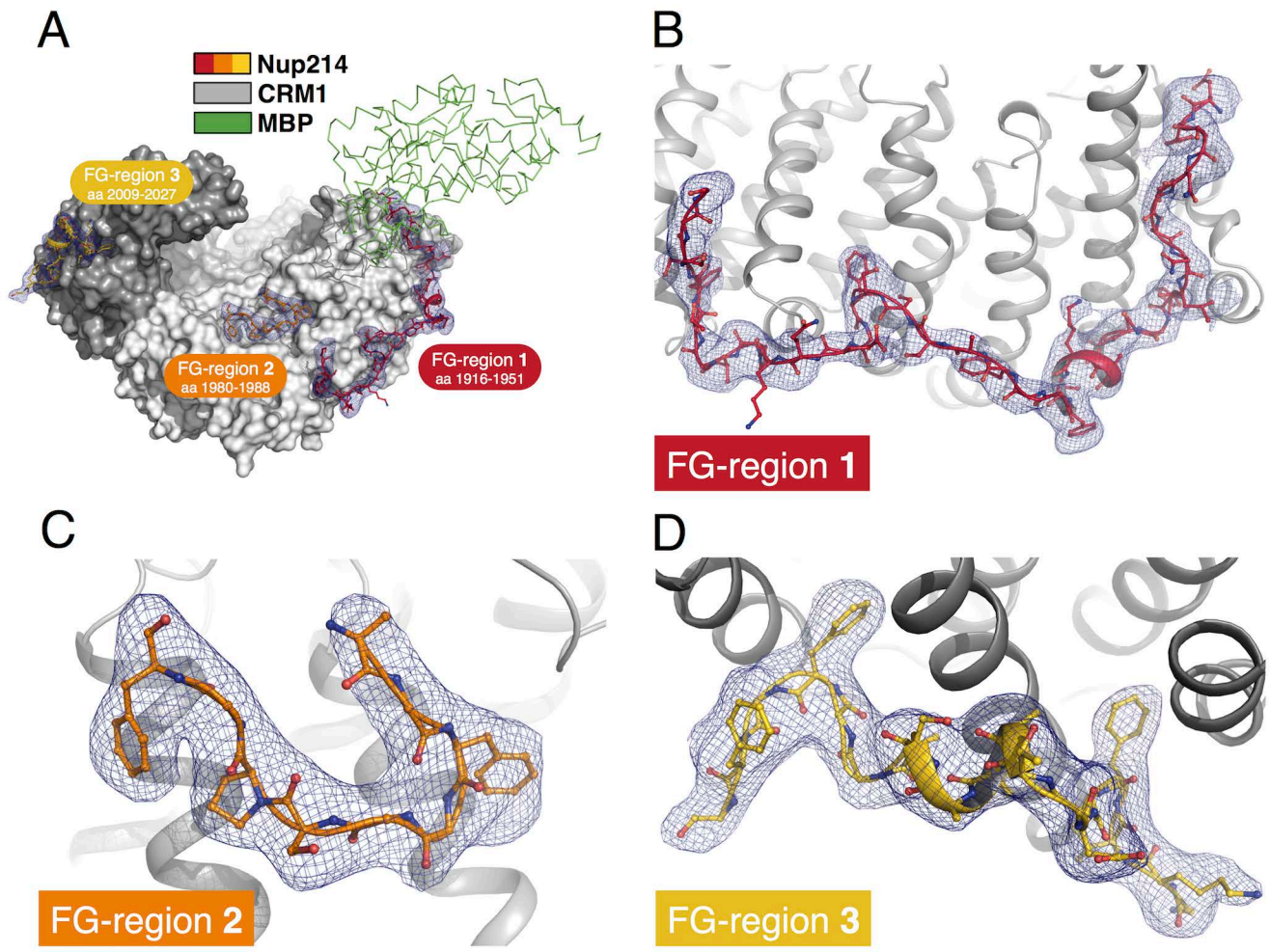
A
Nup214
CRM1
MBP
FG-region 3
aa 2009-2027
FG-region 2
aa 1980-1988
FG-region 1
aa 1916-1951
B
FG-region 1
C
FG-region 2
D
FG-region 3

Figure S3

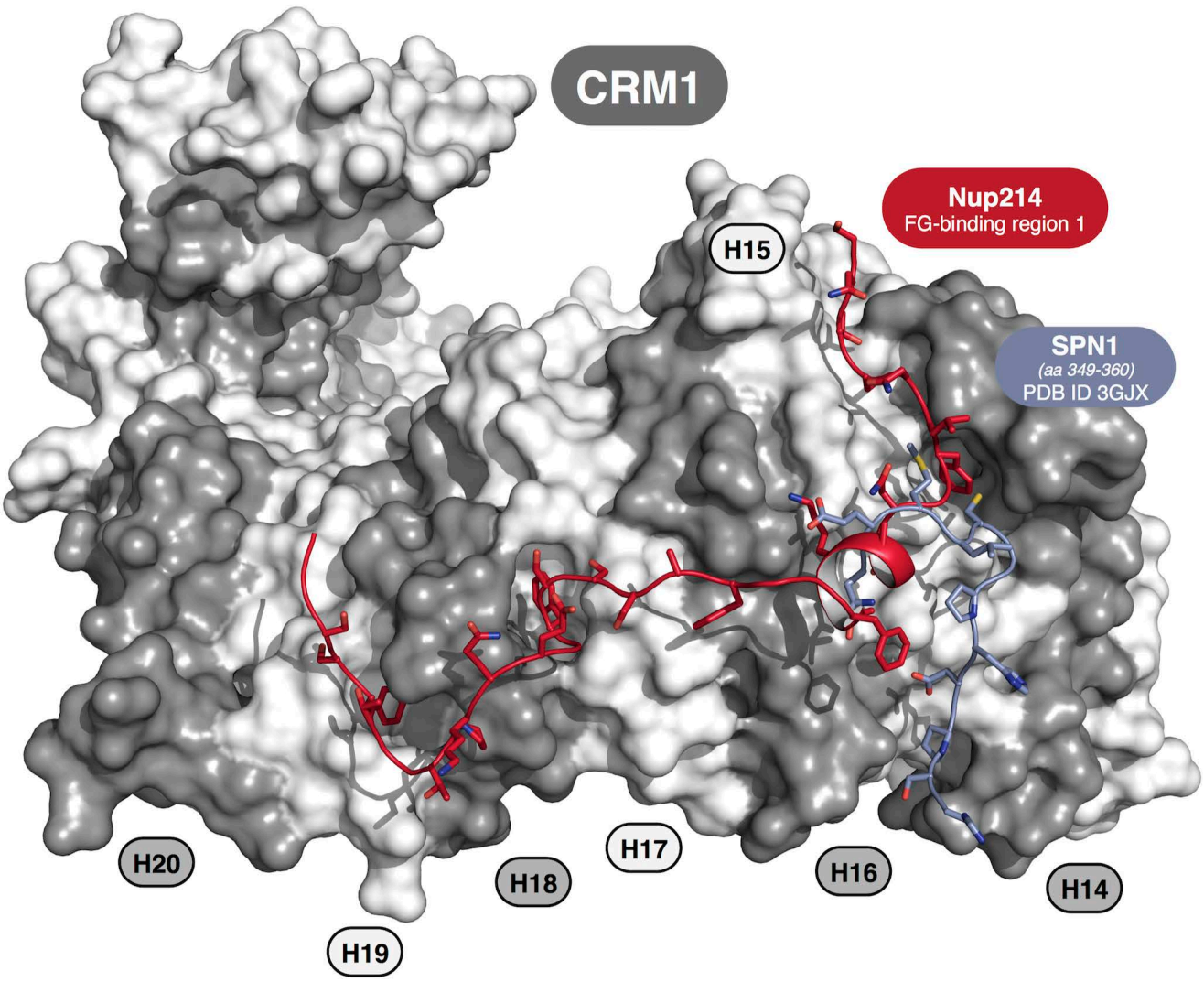
CRM1
Nup214
FG-binding region 1
H15
SPN1
(aa 349-360)
PDB ID 3GJX
H20
H19
H18
H17
H16
H14

Figure S4

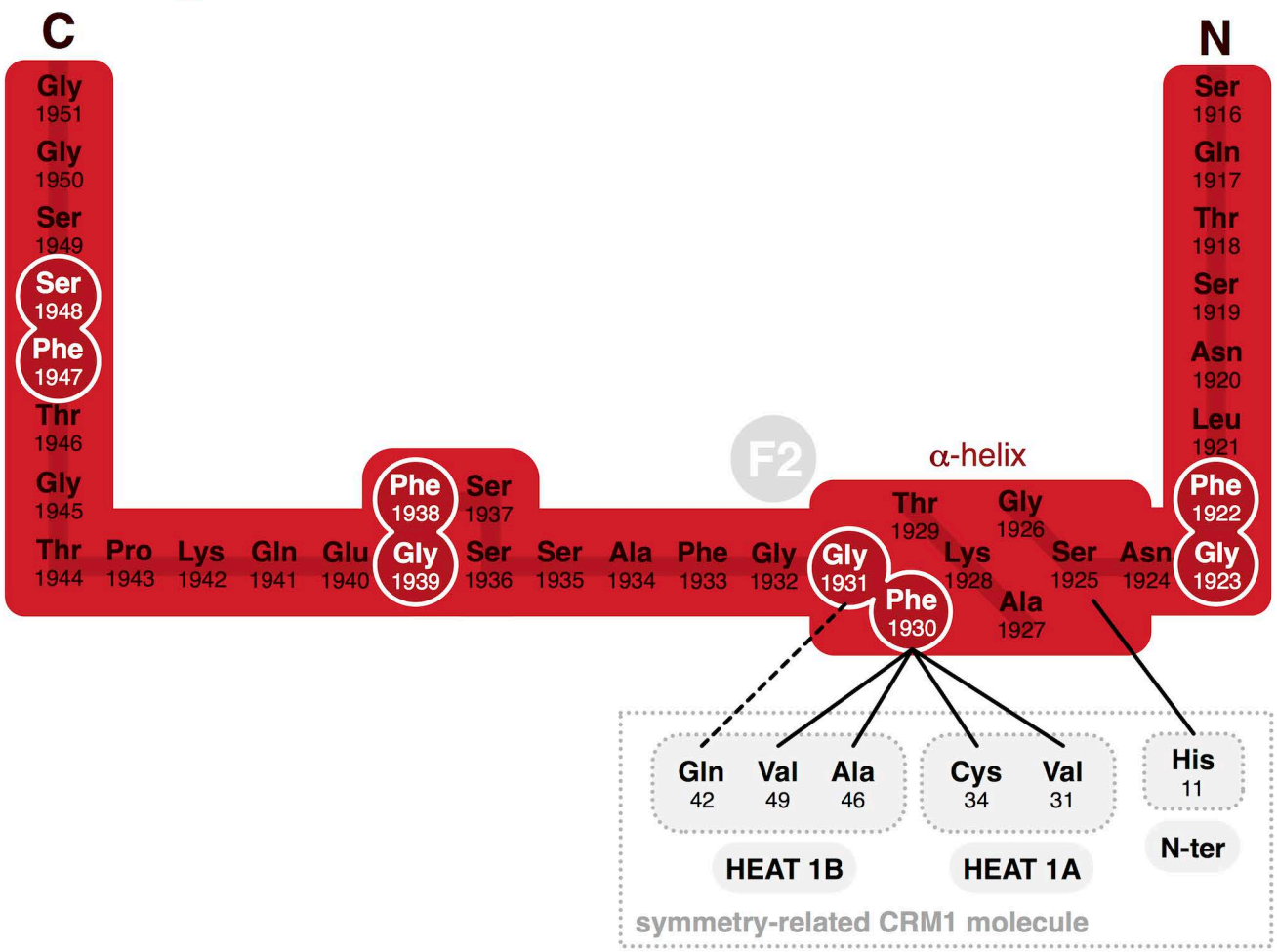
FG-region 1
C
N
Gly 1951
Gly 1950
Ser 1949
Ser 1948
Phe 1947
Thr 1946
Gly 1945
Thr 1944
Pro 1943
Lys 1942
Gln 1941
Glu 1940
Phe 1938
Gly 1939
Ser 1937
Ser 1936
Ser 1935
Ala 1934
Phe 1933
Gly 1932
F2
α-helix
Gly 1931
Phe 1930
Thr 1929
Lys 1928
Ala 1927
Gly 1926
Ser 1925
Asn 1924
Ser 1916
Gln 1917
Thr 1918
Ser 1919
Asn 1920
Leu 1921
Phe 1922
Gly 1923
Gln 42
Val 49
Ala 46
Cys 34
Val 31
His 11
N-ter
HEAT 1B
HEAT 1A
symmetry-related CRM1 molecule

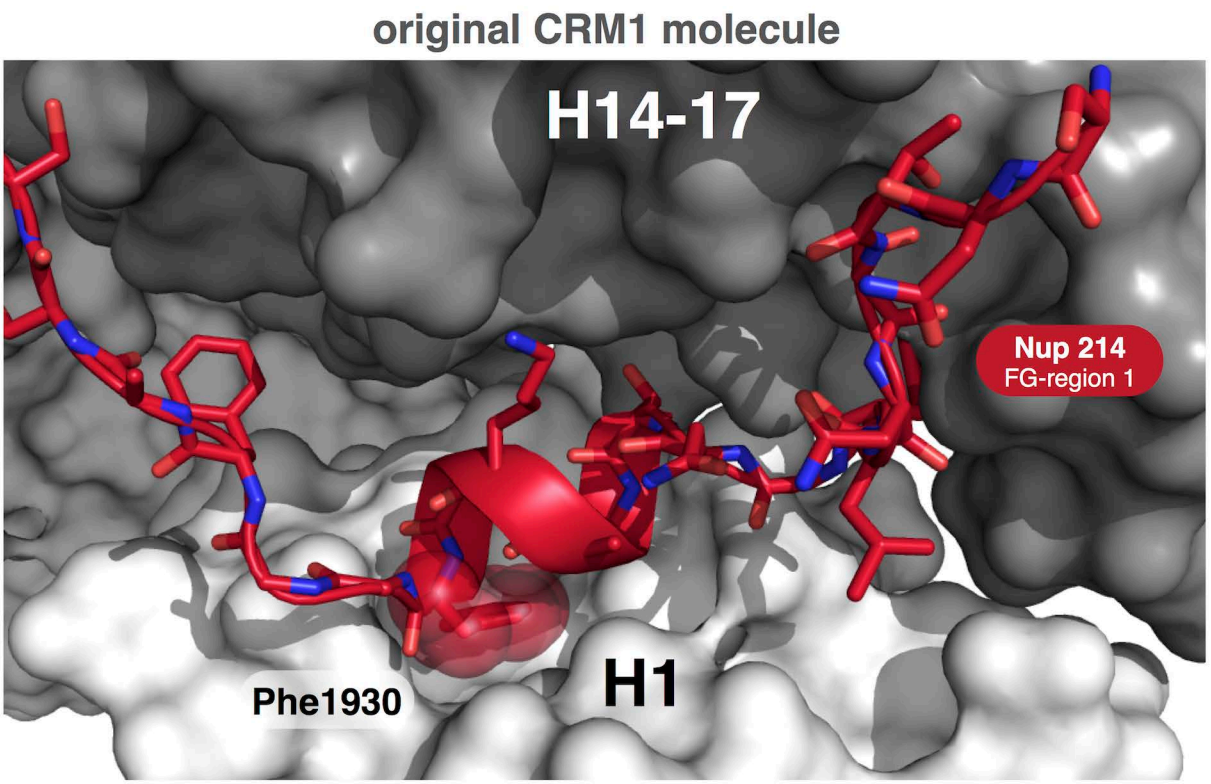
original CRM1 molecule
H14-17
Nup 214
FG-region 1
Phe1930
H1
symmetry-related CRM1 molecule

Figure S5

A

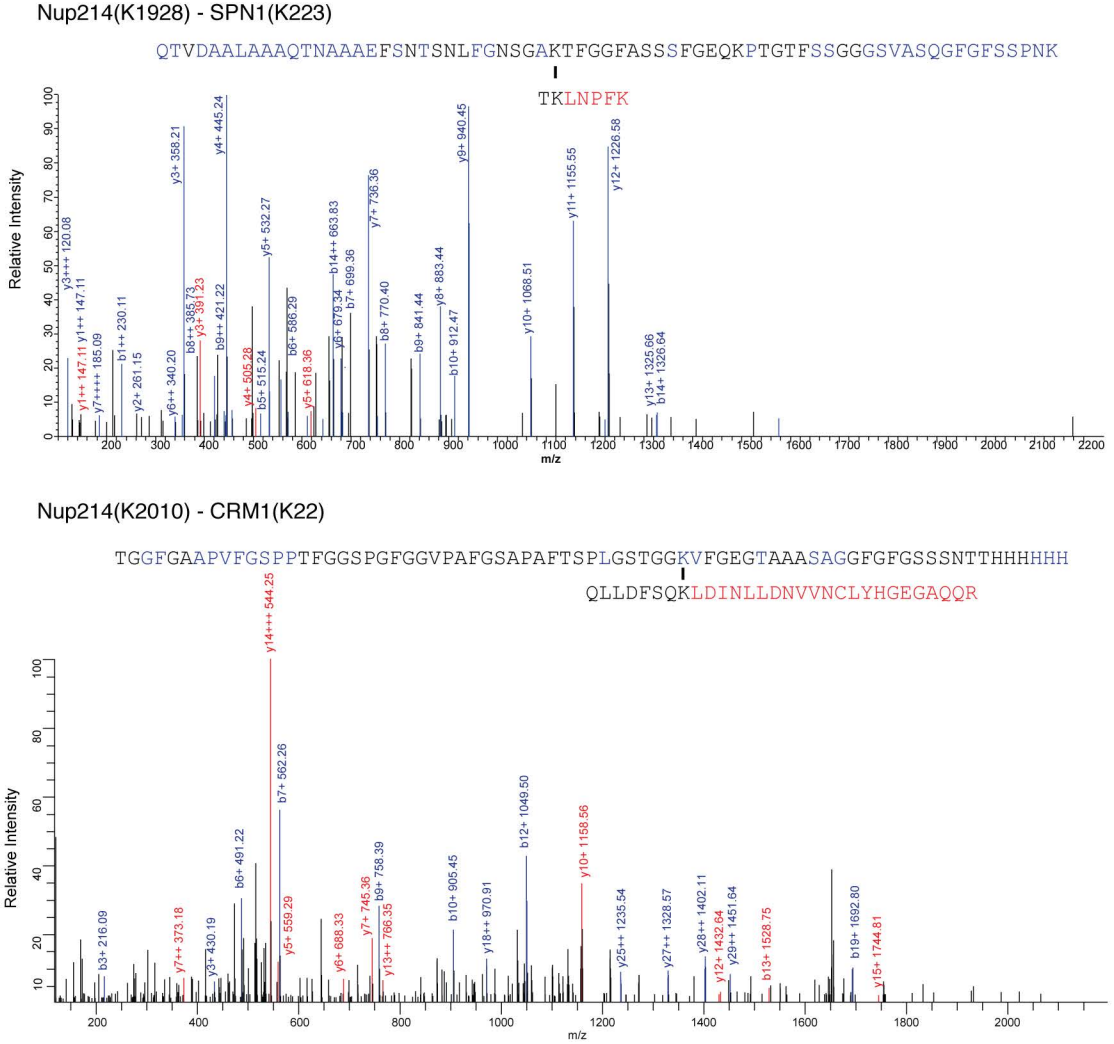
Nup214(K1928) - SPN1(K223)
QTVDAALAAAQTNAAAEFSNTSNLFGNSGAKTFGGFASSSFGEQKPTGTFSSGGGSVASQGFGFSSPNK
TKLNPFK
Relative Intensity
m/z
Nup214(K2010) - CRM1(K22)
TGGFGAAPVFGSPPTFGGSPGFGGVPAFGSAPAFTSPLGSTGGKVFGEGTAAASAGGFGFGSSSNTTHHHHHH
QLLDFSQKLDINLLDNVVNCLYHGEGAQQR
Relative Intensity
m/z

B

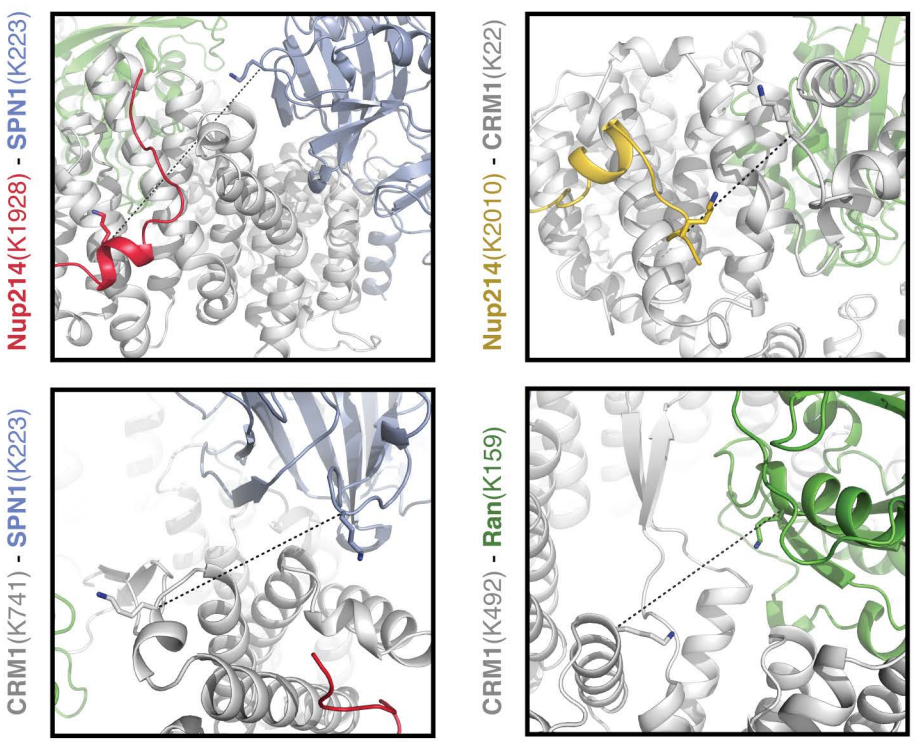
Nup214(K1928) - SPN1(K223)
Nup214(K2010) - CRM1(K22)
CRM1(K741) - SPN1(K223)
CRM1(K492) - Ran(K159)

Figure S6

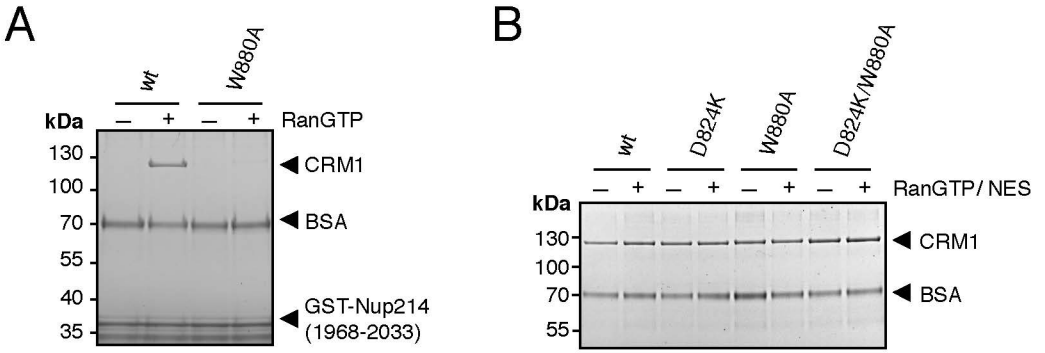
A
wt
W880A
kDa
– + – +
RanGTP
130
100
70
55
40
35
CRM1
BSA
GST-Nup214
(1968-2033)
B
wt
D824K
W880A
D824K/W880A
kDa
– + – + – + – +
RanGTP/ NES
130
100
70
55
CRM1
BSA

Supplemental Figure Legends

Figure S1: Size exclusion chromatography of the Nup214 export complex and analysis of protein crystals; related to Experimental Procedures.

(A) Chromatogram of a Superdex 200 gel filtration run after assembly of CRM1, MBP-Nup214$_{1916\text{-}2033}$, RanGTP$_{1\text{-}180,\ Q69L}$ and SPN1$_{1\text{-}291}$. Peak 1 corresponds to the tetrameric complex (compare B, prep), peaks 2, 3 and 4 to excess Nup214, SPN1 and RanGTP, respectively. In the presence of RanGDP instead of RanGTP, no stable complex was formed (data not shown). For SDS-PAGE (B), several crystals (C) were washed (wash) and dissolved (crystal). Proteins were analyzed on a 4-20% gradient gel with subsequent Coomassie staining. Note that all protein components (CRM1, MBP-Nup214, RanGTP and SPN1) are present in the crystals and no significant degradation is observed upon crystallization.

Figure S2: Simulated annealing omit maps for Nup214 FG-regions 1-3 and location of MBP; related to Figure 2.

(A) Representative mFo-DFc simulated annealing electron density omit maps (blue mesh) for individual parts of Nup214 (red, orange or yellow) omitted, as calculated by CNS (Brünger et al., 2007). CRM1 is depicted as surface and gradient colored from grey to white from N- to C-terminus. Nup214 residues are shown as sticks and electron density maps are contoured at a σ-level of 3.0. MBP (green ribbon) was fused to the N-terminus of the Nup214 fragment for crystallization. Detail views on individual FG-regions for Nup214 residues 1916-1951 (FG-region 1) omitted (B), residues 1980-1988 (FG-region 2) omitted (C) and residues 2009-2027 (FG-region 3) omitted (D). CRM1 is depicted in cartoon mode and colored as in A.

Figure S3: Binding sites for the SPN1 C-terminal residues in the ternary export complex and residues of Nup214 FG-repeats (FG-motifs 1-2) on CRM1 partially overlap; related to Figure 2.

CRM1 is shown as surface model and the HEAT repeats (H14-H20) are colored alternating in grey and white. Nup214 residues 1916-1951 bound to the FG-binding patch 1 of CRM1 are depicted in red, while the C-terminal residues of SPN1 bound to the same CRM1 region from the ternary export complex (PDBid 3gjx) are colored in blue. Note that the binding sites for both molecules partially overlap on CRM1.

Figure S4: FG-motif 2 interacts with an FG-binding pocket at the N-terminus of a symmetry-related CRM1 molecule; related to Figures 2, 3.

(A) Schematic representation of the interaction between Nup214 in red (1916-1951) and CRM1. The original CRM1 molecule is shown in grey, while the symmetry-related CRM1 molecule contributing the FG-binding pocket for FG-motif 2 (F2) is depicted in white. Polar interactions are represented as dashed lines (≤ 3.5 Å) while hydrophobic and van-der-Waals interactions are depicted as solid lines (≤ 4 Å). N- and C-termini as well as α-helical regions are labeled. FG-motifs are encircled in white and highlighted. (B) Structural representation showing binding of FG-motif 2 (red) to the symmetry-related CRM1 molecule (white surface). Phenylalanine 1930 of the FG-repeat is illustrated by transparent spheres and labeled.

Figure S5: Protein-protein cross-linking within the trimeric export complex with bound Nup214; related to Figure 3.

(A) MSMS analyses of cross-linked peptides derived from Nup214 and SPN1 (Nup214 K1928 – SPN1 K223) and CRM1 (Nup214 K2010 – CRM1 K22). See also Supplementary

Tables S1 and S2. The sequences of the cross-linked peptides are shown with their respective b-and y-type fragment ions in the spectra. (B) Examples of protein-protein cross-links visualized in the 3D structure of the protein complex.

Figure S6: CRM1 (D824K/W880A) double FG-binding pocket mutant; related to Figure 5.

Pull-downs. (A) 50 pmol GST-Nup214$_{1968\text{-}2033}$ was immobilized on beads and incubated with 50 pmol of wild type CRM1 or the CRM1 (W880A) mutant and NES peptide in the absence or presence of 150 pmol RanGTP$_{Q69L}$. Bound proteins were analyzed by SDS-PAGE, followed by Coomassie-staining. (B) 25 pmol of the respective CRM1 mutants were incubated with phenylsepharose in the absence or presence of 75 pmol RanGTP and 2.5 μM NES peptide. Bound proteins were analyzed by SDS-PAGE, followed by Coomassie-staining.

Table S1: **X-ray data collection, refinement and validation statistics for the Nup214 export complex**; related to Figure 2

Data collection	
Space group	$C222_1$
Number of complexes in a. u.	1
Wavelength, Å	0.9184
Cell dimensions	
a, *b*, *c;* Å	112.33, 248.97, 210.57
α, β, γ; °	90.0, 90.0, 90.0
Resolution, Å	48.49-2.85 (2.95-2.85)*
R_{merge}	0.055 (0.571)
R_{meas}	0.062 (0.644)
$CC_{1/2}$	99.9 (87.3)
$I/\sigma(I)$	15.52 (2.01)
Completeness, %	98.2 (91.4)
Multiplicity	4.6 (4.1)
Refinement	
Resolution, Å	30.00-2.85
No. reflections	67922
R_{work}	0.205
R_{free}	0.249
No. atoms	14991
B-factor, $Å^2$	125.0
r.m.s.d.	
Bond lengths, Å	0.006
Bond angles, °	0.925

* Values in parentheses indicate the specific values in the particular highest resolution shell.

Table S2: intraprotein cross-links; related to Figure 3

Protein	Peptide 1	Peptide 2	Residue 1	Residue 2	Distance 3GJX	Distance
SPN1	RLAEDDWTGMESEEENKK	DDEEMDIDTVKKLPK	80	93	ND	ND
SPN1	QTHYSPGSTPLVGWLRPYMVSDVLGVAVPAGPLTTKP DYAGHQLQQIMEHK	KSQK	298	314	ND	ND
SPN1	NSTAKDYTILDCIYNEVNQTYYVLDVMCWR	FYWMHSKLPEEEGLGEK	167	211	17.5	18.1
SPN1	LTHKASENGHYELEHLSTPK	TKLNPFK	327	223	ND	ND
SPN1	ASENGHYELEHLSTPKLK	TKLNPFK	343	223	ND	ND
SPN1	ASENGHYELEHLSTPKLK	LLELQKSK	343	52	ND	ND
SPN1	ASENGHYELEHLSTPKLK	LSQYKSK	343	32	ND	ND
SPN1	SKYSSLEQSER	LLELQKSK	34	52	29.0	30.6
SPN1	LSQYKSK	EKLTHK	32	323	ND	ND
SPN1	GSTSAYTKSGYCVNR	LSQYKSK	144	32	ND	ND
SPN1	LLELQKSK	EKLTHK	52	323	ND	ND
SPN1	GSTSAYTKSGYCVNR	SKYSSLEQSER	144	34	24.6	23.5
SPN1	LSQYKSK	KSQK	32	314	ND	ND
SPN1	LSQYKSK	KLPK	32	93	ND	ND
SPN1	GSTSAYTKSGYCVNR	KSQK	144	314	ND	ND
SPN1	LLELQKSK	KSQK	52	314	ND	ND
SPN1	LLELQKSK	KLPK	52	93	14.4	14.7
SPN1	TKLNPFK	KSQK	223	314	ND	ND
CRM1	LHNQVNGTEWSWKNLNTLCWAIGSISGAMHEEDEK	FLVTVIKDLLGLCEQKR	492	522	20.7	20.5
CRM1	ACKAVGHPFVIQLGR	ETLKLISGWVSR	700	757	10.0	10.2
CRM1	QEWPKHWPTFISDIVGASR	LLSEEVFDFSSGQITQVKSK	144	190	12.1	11.8
CRM1	ACKAVGHPFVIQLGR	QLGSILKTNVR	700	693	10.7	10.7
CRM1	ACKAVGHPFVIQLGR	EFMKDTDSINLYK	700	446	18.5	17.6
CRM1	VDTILEFSQNMNTKYYGLQILENVIK	TSSDPTCVEKEK	76	122	11.1	12.1
CRM1	MAQEVLTHLKEHPDAWTR	YYGLQILENVIKTR	54	88	16.4	13.0
CRM1	NLNTLCWAIGSISGAMHEEDEKR	AHWKFLK	514	560	14.4	14.6
CRM1	QEWPKHWPTFISDIVGASR	WKILPR	144	92	12.6	12.9
CRM1	QLLDFSQKLDINLLDNVVNCLYHGEGAQQR	MPAIMTMLADHAAR	22	1	ND	ND
CRM1	ACKAVGHPFVIQLGR	IAQKCR	700	594	15.4	15.5
CRM1	EFMKDTDSINLYK	IAQKCR	446	594	19.5	19.1
CRM1	ETLKLISGWVSR	QLGSILKTNVR	757	693	9.0	9.0
CRM1	FLVTVIKDLLGLCEQK	GKDNK	522	534	19.4	19.4
CRM1	NVDILKDPETVK	QLGSILKTNVR	680	693	18.7	19.2
CRM1	LLSEEVFDFSSGQITQVKSK	WKILPR	190	92	14.1	14.8
CRM1	YYGLQILENVIKTR	WKILPR	88	92	8.9	9.3
CRM1	QADEEKHKR	SKHLK	1049	192	24.3	ND
CRM1	FLVTVIKDLLGLCEQK	AHWKFLK	522	560	15.6	15.8
CRM1	ETLKLISGWVSR	TVKR	757	752	8.7	8.7
CRM1	QADEEKHKR	IAQKCR	1049	594	53.2	ND
CRM1	DTDSINLYKNMR	IAQKCR	455	594	20.2	20.0
CRM1	DLLGLCEQKR	GKDNK	531	534	8.8	8.9
RAN	NLQYYDISAKSNYNFEKPFLWLAR	VCENIPIVLCGNKVDIKDR	152	127	12.7	12.9
RAN	NLQYYDISAKSNYNFEKPFLWLAR	HLTGEFEKK	152	37	8.8	9.2
RAN	VCENIPIVLCGNKVDIKDR	KVKAK	127	132	11.6	11.4
RAN	KYVATLGVEVHPLVFHTNR	TTFVKR	38	28	12.1	11.9
RAN	VTYKNVPNWHR	AKSIVFHR	99	134	14.1	14.1
RAN	VCENIPIVLCGNKVDIK	DRKVK	123	130	10.6	10.7
RAN	VTYKNVPNWHR	KVKAK	99	132	12.8	12.6
RAN	VTYKNVPNWHR	KNLQYYDISAK	142	99	14.8	14.9
RAN	HLTGEFEKK	TTFVKR	37	28	11.1	11.3

Table S3: interprotein cross-links; related to Figure 3

Protein 1	Protein 2	Peptide 1	Peptide 2	Residue 1	Residue 2	Distance
SPN1	CRM1	QLYLPMLFKVR	LSQYKSK	32	415	ND
RAN	CRM1	NLQYYDISAKSNYNFEKPFLWLAR	ETLKLISGWVSR	152	757	20.3
RAN	CRM1	VCENIPIVLCGNKVDIKDR	ACKAVGHPFVIQLGR	127	700	17.7
RAN	CRM1	VCENIPIVLCGNKVDIKDR	ETLKLISGWVSR	127	757	16.8
RAN	CRM1	VTYKNVPNWHR	QADEEKHKR	99	1049	ND
SPN1	CRM1	LAEDDWTGMESEEENKKDDEEMDIDTVK	DLLGLCEQKRGK	81	531	ND
SPN1	CRM1	TKLNPFKFVGLK	NVDILKDPETVK	223	680	10.5
SPN1	RAN	LPEEEGLGEKTKLNPFK	SNYNFEKPFLWLAR	221	159	48.4
CRM1	RAN	LHNQVNGTEWSWKNLNTLCWAIGSISGAMHEEDEKR	SNYNFEKPFLWLAR	492	159	21.3
CRM1	RAN	LFVTGLFSLNQDIPAFKEHLRDFLVQIK	VTYKNVPNWHR	1012	99	16.0
CRM1	SPN1	YMLLPNQVWDSIIQQATKNVDILKDPETVK	TKLNPFK	674	223	17.2
CRM1	RAN	LAYSNGKDDEQNFIQNLSLFLCTFLKEHDQLIEK	AKSIVFHR	331	134	16.5
CRM1	RAN	RETLKLISGWVSR	HLTGEFEKK	757	37	20.6
CRM1	RAN	CLSENISAAIQANGEMVTKQPLIR	HLTGEFEKK	741	37	15.1
CRM1	SPN1	NVDILKDPETVKQLGSILK	TKLNPFK	686	223	14.9
CRM1	SPN1	LHNQVNGTEWSWKNLNTLCWAIGSISGAMHEEDEKR	KLPK	492	93	29.1
CRM1	RAN	MAKPEEVLVVENDQGEVVR	SNYNFEKPFLWLAR	426	159	18.2
CRM1	SPN1	FLVTVIKDLLGLCEQKR	LSQYKSK	522	32	ND
CRM1	SPN1	FLVTVIKDLLGLCEQKR	SKYSSLEQSER	522	34	ND
CRM1	SPN1	AHWKFLK	LSQYKSK	560	32	ND
CRM1	SPN1	CLSENISAAIQANGEMVTKQPLIR	TKLNPFK	741	223	20.9
CRM1	SPN1	FLKTVVNK	LSQYKSK	563	32	ND
CRM1	SPN1	GKDNK	KLPK	534	93	14.7
NUP	SPN1	QTVDAALAAAQTNAAAEFSNTSNLFGNSGAKTFGGFA SSSFGEQKPTGTFSSGGGSVASQGFGFSSPNK	TKLNPFK	1928	223	31.8
NUP	CRM1	TGGFGAAPVFGSPPTFGGSPGFGGVPAFGSAPAFTSP LGSTGGKVFGEGTAAASAGGFGFGSSSNTTHHHHHH	QLLDFSQKLDINLLDNVVNCLYHGEGAQQR	2010	22	14.2
SPN1	CRM1	DLLGLCEQKR	KLPK	93	531	20.5

Table S4: Plasmids generated in this study; related to Experimental Procedures

Plasmid	Cloning
pQE60-CRM1 (A156F)-His	mutagenesis on pQE60-CRM1-His (5'-cttttatcagtgatattgttggaTTTagtaggaccagcgaaagtctc-3'/ 5'-gagactttcgctggtcctactAAAtccaacaatatcactgataaaag-3')
pQE60-CRM1 (L679R)-His	mutagenesis on pQE60-CRM1-His (5'-caaccaaaaatgtggatataCGTaaagatcctgaaacagtcaagcag-3'/ 5'-ctgcttgactgtttcaggatctttACGtatatccacatttttggttg-3')
pQE60-CRM1 (D824K)-His	mutagenesis on pQE60-CRM1-His (5'-ctgaaatacctcaaatatttAAAgctgtttttgaatgcacattg-3'/ 5'-caatgtgcattcaaaaacagcTTTaaatatttgaggtatttcag-3')
pQE60-CRM1 (Y918W)-His	mutagenesis on pQE60-CRM1-His (5'-ctcagagtttttatcaaactTGGttttgtgatattctccagcata-3'/ 5'-tatgctggagaatatcacaaaaCCAagtttgataaaaaactctgag-3')
pQE60-CRM1 (W880A)-His	mutagenesis on pQE60-CRM1-His (5'-cttgttttggattccatcattGCGgctttcaaacatactatgag-3'/ 5'-ctcatagtatgtttgaaagcCGCaatgatggaatccaaaacaag-3')
pQE60-CRM1 (S928K)-His	mutagenesis on pQE60-CRM1-His (5'-gatattctccagcatatctttAAGgttgtgacagacacttcac-3'/ 5'-gtgaagtgtctgtcacaacCTTaaagatatgctggagaatatc-3')
pQE60-CRM1 (D824K/W880A)-His	mutagenesis on pQE60-CRM1 (D824K)-His (5'-cttgttttggattccatcattGCGgctttcaaacatactatgag-3'/ 5'-ctcatagtatgtttgaaagcCGCaatgatggaatccaaaacaag-3')
pQE60-CRM1 (A156F/D824K/W880A)-His	mutagenesis on pQE60-CRM1 (D824K/W880A)-His (5'-cttttatcagtgatattgttggaTTTagtaggaccagcgaaagtctc-3'/ 5'-gagactttcgctggtcctactAAAtccaacaatatcactgataaaag-3')
pGEX-Nup214(1859-2090)	PCR Nup214 (5'-tttGAATTCggaatagtctttggccagcaatcatcct-3'/ 5'-tttGTCGACtcagcttcgccagccaccaaaac-3'), cloned into pGEX-6P1 (EcoRI, SalI)
pGEX-Nup214(1930-2021)	PCR Nup214 (5'-tttGAATTCtttggtggatttgccagctcgtcg-3'/ 5'-tttGTCGACttatgcgctggcagctgcagtg-3'), cloned into pGEX-6P1 (EcoRI, SalI)
pmRFP-Nup214(1859-2090)-cNLS	PCR Nup214 (5'-tttGAATTCcggaatagtctttggccagca-3'/ 5'-tttGTCGACgcttcgccagccaccaaa-3'), cloned into pmRFP-cNLS (Roloff et al., 2013) (EcoRI, SalI)
pmRFP-Nup214(1859-2090)X1/X2/X3-cNLS	synthesized fragments cloned into pmRFP-cNLS (Roloff et al., 2013) (EcoRI, SalI)
pET28a-His-Nup214(1916-2033)X1/X3-His	PCR on pmRFP-Nup214(1859-2090)X1/X3-cNLS plasmids (5'-tttCATATGtcaaatacctctaacctatctggaaacag-3'/ 5'-tttCTCGAGtgtggtgttgctgctgctcc-3'), cloned into pET28a (NdeI, XhoI)
pET28a-His-Nup214(1916-2033)X2-His	PCR on pmRFP-Nup214(1859-2090)X2-cNLS plasmid (5'-tttCATATGtcaaatacctctaacctatttggaaacag-3'/ 5'-tttCTCGAGtgtggtgttgctgctgctcc-3'), cloned into pET28a (NdeI, XhoI)
pMal-linkerAAA	PCR on pMal-c2 (5'-tttAGATCTgctgccgaacccgccaaaaacctgg-3'/ 5'-aatGAATTCggccgcggcattagtctgcgcggctgccagggctgcatcgacagtc-3'), cloned into pMal-c2 (BglII, EcoRI)
pMal-linkerAAA-Nup214(1916-2033)X1/X3-His	PCR on pmRFP-Nup214(1859-2090)X1/X3-cNLS plasmids (5'-tttGAATTCtcaaatacctctaacctatctggaa-3'/ 5'-tttGTCGACttagtgatggtgatggtgatgtgtggtgttgctgctgctcc-3'), cloned into pMal-linkerAAA (EcoRI/SalI)
pMal-linkerAAA-Nup214(1916-2033)X2-His	PCR on pmRFP-Nup214(1859-2090)X2-cNLS plasmid (5'-tttGAATTCtcaaatacctctaacctatttggaa-3'/5'-tttGTCGACttagtgatggtgatggtgatgtgtggtgttgctgctgctcc-3'), cloned into pMal-linkerAAA (EcoRI/SalI)
pMal-linkerAAA-Nup214(1916-2033)-His	PCR Nup214 (5'-tttGAATTCtcaaatacctctaacctatttggaa-3'/ 5'-tttGTCGACttagtgatggtgatggtgatgtgtggtgttgctgctgctcc-3'), cloned into pMal-linkerAAA (EcoRI/SalI)
pMal-linkerAAA-Nup214(1930-2021)-His	PCR Nup214 (5'-tttGAATTCtttggtggatttgccagctcgtcg-3'/ 5'-tttGTCGACttatgcgctggcagctgcagtg-3'), cloned intopMal-linkerAAA (EcoRI/SalI)
pGEX-Nup62	PCR Nup62 (5'-aaaGTCGACaaatgagcgggtttaattttggag-3'/ 5'-aaaGCGGCCGCtcagtcaaaggtgatccgga-3'), cloned into pGEX-6P1 (NotI/SalI)
pGEX-RanBP3	cloned into pGEX-6P1 (BamHI/XhoI)

Supplemental Table Legends

Table S1: X-ray data collection, refinement and validation statistics for the Nup214 export complex; related to Figure 2.

Table S2 and S3: Intra- and Interprotein cross-links identified in the trimeric export complex with bound Nup214; related to Figure 3.

Protein-protein cross-links identified in the trimeric export complex with bound Nup214. The intra- (S1) and inter- (S2) cross-linked peptides with their respective cross-linked lysine residues are listed. The distances in Å according to the crystal structure are also listed. ND: not determined, as these parts are missing in the crystal structure. *, cross-links with distances >30 Å. These can be explained by the flexibility of the involved regions. For example, Lys1049 (crosslinking to $Lys594^{CRM1}$) is located in the C-terminal helix 21B of CRM1, which is known to adopt various orientations in different crystal structures. Lysine 221 of SPN1 (crosslinking to $Lys159^{Ran}$) is located in a loop region with increased flexibility, as reflected by its elevated B-factors. This is indicative of a high flexibility of the whole SPN1 loop 215-228 in the context of the export complex in solution.

Table S4: **Plasmids generated in this study**; related to Experimental Procedures.

Supplemental Experimental Procedures

Plasmids

Plasmids coding for CRM1 mutants were obtained by site-directed mutagenesis on the wild type plasmid.

A vector pMal-linkerAAA was cloned from the pMal-c2 vector with appropriate primers to resemble a previously published vector (Smyth et al., 2003).

Nup214-fragments were amplified by PCR and cloned into pMal-linkerAAA, pGEX-6P1 and pmRFP-cNLS (Roloff et al., 2013) *via* EcoRI/SalI.

Coding sequences for $Nup214_{1859-2090}$-X1/X2/X3 mutants were synthesized (GeneArt) and cloned into pmRFP-cNLS (Roloff et al., 2013) *via* EcoRI/SalI. Coding sequences for His-$Nup214_{1916-2033}$ and MBP-$Nup214_{1916-2033}$ mutants were amplified from the respective pmRFP-$Nup214_{1859-2090}$-cNLS plasmids and cloned into pET28a and pMal-linkerAAA *via* NdeI/XhoI and EcoRI/SalI, respectively.

The coding sequences of RanBP3 (isoform b) and Nup62 were amplified by PCR and cloned into pGEX-6P1 *via* BamHI/XhoI or NotI/SalI, respectively.

Further details about sequences and primers can be found in Table S3.

Protein Expression and Purification

Expression and purification of CRM1 (Dolker et al., 2013; Guan et al., 2000), importin β (Chi et al., 1997), importin 5 (Jäkel and Görlich, 1998), importin 13 (Mingot et al., 2001), transportin (Baake et al., 2001), RanGAP (Mahajan et al., 1997), Ran (Melchior et al., 1995), GST-SPN1 (Strasser et al., 2004), His-SPN1 (Waldmann et al., 2012), GST-Rev (Arnold et al., 2006), GST-Nup214 and His-$Nup214_{1916-2033}$ (Roloff et al., 2013) was adapted from published protocols.

CRM1 mutants were expressed in *E. coli* TG1 cells in 2YT medium supplemented with ampicillin. Cells were grown at 37 °C to an OD_{600} of 0.7. Protein expression was induced by adding 0.1 mM IPTG and cells were grown at 37 °C for 5 hours. Cells were harvested (5000 xg, 20 minutes, 4 °C), washed with PBS and stored at -80 °C until purification. CRM1 mutants were purified as described for wild type CRM1.

H. sapiens His_{10}ZZ-[TEV]-$RanGTP_{1\text{-}180,\,Q69L}$ (Monecke et al., 2009) was expressed in *E. coli* BL21(DE3)pLysS in 2YT medium supplemented with ampicillin, chloramphenicol and 2% (w/v) α-D-glucose to repress basal expression. Cells were grown at 37 °C to an optical density (OD_{600}) of 0.4 and temperature was gradually reduced to 18 °C in three steps. Protein expression was induced at an OD_{600} of 0.9 adding IPTG to a final concentration of 0.5 mM. Cells were harvested after 15 h of induction (5000 xg, 20 minutes, 4 °C) and resuspended in lysis buffer (500 mM NaCl, 50 mM HEPES/NaOH pH 7.0, 5 mM $MgCl_2$, 3 mM imidazole, 10% (v/v) glycerol, 50 μM GTP and 1 mM DTT). Cells were disrupted using a Microfluidizer 110S (Microfluidics), and the clarified lysate (30,000 xg, 30 min, 4 °C) was applied onto a HisTrap column (GE Healthcare) equilibrated with lysis buffer. Unbound proteins were removed by washing with two column volumes of lysis buffer and bound His_{10}ZZ-RanGTP was eluted with lysis buffer containing 500 mM imidazole. For cleavage, the His_{10}-[TEV]-RanGTP fusion protein was incubated with TEV protease (Invitrogen) at 4 °C overnight in a 100:1 molar ratio. Pooled protein fractions were desalted in lysis buffer and loaded onto a second HisTrap column equilibrated with lysis buffer. The flow through containing RanGTP was collected, concentrated and passed over a Superdex S75 gel filtration column (GE Healthcare) equilibrated with 500 mM NaCl, 50 mM HEPES/NaOH pH 7.0, 5 mM $MgCl_2$, 10% (v/v) glycerol, 30 μM GTP and 1 mM DTT. RanGTP containing fractions were pooled, concentrated, frozen in liquid nitrogen and stored at –80 °C.

Expression and purification of *H. sapiens* $SPN1_{1\text{-}291}$ was analogous to full-length SPN1 (Strasser et al., 2004).

GST-Nup214 and His-Nup214 fragments were expressed and purified as described before (Roloff et al., 2013). Glutathione was removed from the eluted GST-Nup214 by buffer exchange into GST prep buffer (50 mM Tris pH 6.8, 300 mM NaCl, 1 mM $MgCl_2$, 0.25 mM EDTA, 1 mM DTT, 1 μg/ml each of leupeptin, pepstatin, and aprotinin) with PD-10 Desalting Columns (GE Healthcare). His-Nup214 fragments were additionally purified with a HiLoad 26/60 Superdex 75 prep grade column (GE Healthcare) in His prep buffer (50 mM Tris pH 6.8, 200 mM NaCl, 1 mM $MgCl_2$, 10% glycerol, 4 mM β-mercaptoethanol, 0.1 mM PMSF and 1μg/ml each of leupeptin, pepstatin, and aprotinin). The fractions containing the His-Nup214 were determined via SDS-PAGE, pooled and concentrated with 20 ml/5 kDa MWCO Spin-XR concentrators (Corning).

Plasmids coding for $_{MBP}$Nup214$_{His}$-fragments contained a C-terminal His_6-tag and an N-terminal modified MBP-tag (Smyth et al., 2003). $_{MBP}$Nup214$_{His}$-fragments were expressed in *E. coli* BL21 (DE3) codon+ cells in MBP rich medium (1% trypton, 0.5% yeast extract, 0.5% NaCl and 0.2% glucose). Expression was induced with 300 μM IPTG and cells were grown overnight at 18 °C. $_{MBP}$Nup214$_{His}$-fragments were purified in His prep buffer (50 mM Tris pH 6.8, 200 mM NaCl, 1 mM $MgCl_2$, 10% glycerol, 4 mM β-mercaptoethanol, 0.1 mM PMSF and 1 μg/ml each of leupeptin, pepstatin, and aprotinin) with a two step protocol using binding to Ni-NTA sepharose followed by binding to amylose resin.

H. sapiens GST-RanBP3 was expressed in *E. coli* Rosetta II (DE3) cells in 2YT medium supplemented with ampicillin, chloramphenicol and 2% glucose. Cells were grown at 37 °C to an OD_{600} of 0.8. Protein expression was induced by adding 0.5 mM IPTG and cells were grown overnight at 18 °C. Cells were harvested (5000 xg, 20 minutes, 4 °C), washed with PBS and stored at -80 °C until purification. Cells were resuspended in RanBP3 buffer (50 mM Tris pH 8.0, 250 mM NaCl, 2 mM $MgCl_2$, 2 mM EDTA, 2mM DTT 1 mM PMSF, 1μg/ml of each leupeptin, pepstatin, and aprotinin) and lyzed using an EmulsiFlex-C3 (Avestin). The clarified lysate (100,000 xg, 30 min, 4 °C) was applied onto glutathion

sepharose (GE Healthcare) equilibrated with RanBP3 buffer at 4 °C for 1 hour. Unbound proteins were removed by three washing steps with RanBP3 buffer and one washing step with RanBP3 buffer supplemented with 1 M LiCl. Bound GST-RanBP3 was eluted with RanBP3 buffer containing 15 mM reduced glutathion. GST-RanBP3 was cleaved with PreScission protease (4 °C, overnight) and purified with a Superdex S200 gel filtration column (GE Healthcare) equilibrated in RanBP3 buffer. RanBP3 containing fractions were pooled, concentrated, frozen in liquid nitrogen and stored at –80 °C.

H. sapiens GST-Nup62 was expressed in *E. coli* BL21 codon+ cells in 2YT medium supplemented with ampicillin. Cells were grown at 37 °C to an OD_{600} of 0.7. Protein expression was induced by adding 0.2 mM IPTG and cells were grown overnight at 18 °C. Cells were harvested (5000 xg, 20 minutes, 4 °C), washed with PBS and stored at -80 °C until purification. Cells were resuspended in Nup62 buffer (50 mM Tris pH 6.8, 300 mM NaCl, 1 mM $MgCl_2$, 5% glycerol, 1 mM DTT, 1 μg/ml each of leupeptin, pepstatin, and aprotinin) supplemented with 1.5% sarkosyl and lyzed using an EmulsiFlex-C3 (Avestin). The clarified lysate (100,000 x g, 30 min, 4 °C) was applied onto glutathion sepharose (GE Healthcare) equilibrated with Nup62 buffer at 4 °C for 1 hour. Unbound proteins were removed by three washing steps with Nup62 buffer and bound GST-Nup62 was eluted with Nup62 buffer containing 15 mM reduced glutathion. GST-Nup62 was either changed into Nup62 buffer without glutathione using PD-10 desalting columns (GE Healthcare) or cleaved with PreScission protease (4 °C, overnight). Cleaved Nup62 was purified with a Superdex S75 gel filtration column (GE Healthcare) equilibrated in Nup62 buffer. Nup62 containing fractions were pooled, concentrated, frozen in liquid nitrogen and stored at –80 °C.

Preparation, crystallization and structure determination of the Nup214 export complex

The CRM1-SPN1-RanGTP-$_{MBP}$Nup214 complex was assembled by mixing the individual components in a 1:3:5:5 molar ratio and subsequently purified using an Superdex 200 gel filtration column (GE Healthcare) in a buffer containing 50 mM NaCl, 20 mM Tris pH 7.5, 2 mM $Mg(OAc)_2$ and 2 mM DTT. The purified complex was concentrated to 5 mg/ml, frozen in liquid nitrogen and stored at -80 °C.

The CRM1-SPN1-RanGTP-$_{MBP}$Nup214$_{1916-2033}$ export complex was crystallized by mixing 2 μl of a 5 mg/ml protein solution with 1 μl of a condition containing 5% (w/v) polyethylene glycol (PEG) 8000, 0.2 M L-proline, 0.1 M Tris/HCl pH 7.5, 4 mM D-maltose and 180 mM LiCl. In order to control the number of crystals per well, several seeds were added to the condition after an incubation time of 20 minutes. Crystals belonging to the orthorhombic space group $C222_1$ grew at 20 °C after 5 days to a typical size of 150 x 150 x 80 μm. After size optimization, crystals diffracted X-rays to a maximum resolution of 7 Å. The diffraction quality could be significantly improved by successive crystal dehydration. For that purpose, crystals were transferred stepwise to conditions with increasing PEG 8,000 concentrations (from 5% to 45% PEG 8,000 with 15 min of incubation between 5% steps). Notably, this treatment did not only improve the diffraction quality of the crystals but additionally resulted in a significant reduction of the unit cell lengths by ≈10% (e.g. a axis from 126 Å to 112 Å (13%), b axis from 263 Å to 248 Å (6%) and c axis from 229 Å to 210 Å (8%). This corresponds to a remarkable decrease in crystal solvent content of 10% (from 69% to 59%). To further improve data quality and reduce scattering contribution from the surrounding liquid (e.g. background noise by the cryo condition) during data collection, the crystals were fished onto micro meshes (MiTeGen) and mounted on beamline 14.3 (BESSY II, Berlin) equipped with an HC1c crystal humidifier. After complete removal of the liquid surrounding the crystal using a paper wick, the crystals were flash cooled in liquid nitrogen and transferred to beamline 14.1 equipped with a 6M Pilatus detector. Complete datasets of two such treated

crystals were collected at beamline 14.1 (BESSY II, Berlin) (Mueller et al., 2012). Data were processed using XDS and XSCALE (Kabsch, 2010).

The structure was solved by means of molecular replacement with PHASER (McCoy et al., 2007) using the export complex CRM1-SPN1-RanGTP (PDBid 3gjx) (Monecke et al., 2009) as a starting model. Subsequently, MBP (PDBid 1anf) (Quiocho et al., 1997) was fitted manually into positive $|F_o-F_c|$ difference density, since localization by molecular replacement routines of PHASER did not provide an unambiguous solution. The poor overall quality of the MBP density suggests that significant movement of MBP in the crystal lattice is possible, which is consistent with the overall elevated B-factors of the MBP residues. Hence, several parts of MBP, especially in its N-terminal lobe, are not defined in the electron density map. However, dissolved crystals analysed by SDS-PAGE clearly showed the presence of full-length MBP. Thus, in order to retain structural integrity of the crystal lattice and the MBP, the residues were not omitted. The final MBP model contains residues 7-112, 115-143, 150-167, 170-173, 176-183, 188-204, 210-224, 229-147 and 257-369.

After replacement and initial rigid body refinement, positive $|F_o-F_c|$ difference electron density near the MBP C-terminus and CRM1 H14-20 as well as at the CRM1 N-terminus (H2-4) allowed us to build three regions of Nup214, each containing a number of canonical FG-repeats. The structure was refined by iterative cycles of CNS (Brunger, 2007) and manual model building in Coot (Emsley et al., 2010). A series of mFo-DFc simulated annealing electron density omit maps as implemented in CNS were used to build the Nup214 sequence as well as ambiguous portions of the other proteins. A final round of refinement was done in Phenix (Adams et al., 2010). Figures were generated with PyMol (The PyMOL Molecular Graphics System, Version 1.5.0.4 Schrödinger, LLC.).

Identification of protein crosslinks by Mass Spectrometry

Tetrameric complexes containing CRM1, SPN1, RanQ69L$_{1-180}$GTP and a MBP-tagged-Nup214$_{1916-2033}$-fragment were assembled and purified by gel filtration in PBS. For crosslinking of 1300 pmol of the Nup214-complex (30 min at 25° C in a total volume of 1.5 mL), a BS3:protein ratio of 200:1 was used. In-solution digestion, reduction and alkylation of BS3 crosslinked complexes were performed as described (De et al., 2015) with minor modifications. Crosslinked complexes were reduced to 50 μL, to which 50 μL 8 M urea in buffer (100 mM phosphate, pH 7.5, 30 min, RT) was added. Reduction and alkylation were achieved by addition of 25 μL 10 mM DTT (Calbiochem):Buffer (50:50, 30 min, RT) and 25 μL of 60 mM IAA:Buffer (50:50, 30 min, RT). Modified trypsin (Promega) was added in a 1:20 w/w ratio for overnight hydrolysis. All reagents were purchased from Sigma-Aldrich, unless otherwise indicated.

The peptide mixture was desalted with C18 Sep Pak columns. Columns were conditioned with 0.4 mL MeOH (Lichrosolv, Merck), 0.5 mL 80% v/v ACN (Lichrosolv, Merck), 0.1% v/v TFA (Roth, Karlsruhe) and 0.5 mL 0.1% TFA. Digests were taken to 5% v/v ACN, 0.1% v/v TFA prior to loading. Column wash was performed with 2X 0.5 mL 0.1% v/v TFA, and elution of peptides was performed with 80% v/v ACN, 0.1% v/v TFA, 2X 0.4 mL. The eluate was dried in a rotary evaporator. Enrichment of crosslinked peptides by size exclusion chromatography (SEC) was performed as reported (Leitner et al., 2012). Peptides were reconstituted in 30% v/v ACN, 0.1% v/v TFA, injected onto a Superdex Peptide column and eluted at 50 μL/min collecting fractions of 50 μL. Fractions 9-18 were dried in a rotatory evaporator and reconstituted in 12 μL LC-MS analysis buffer (5% ACN v/v, 0.1% v/v formic Acid, Fluka, Switzerland) and directly submitted to LC-MS analysis.

Protein-protein cross-linking samples were submitted to LC-MS/MS analysis immediately after their preparation. Protein-protein cross-linking samples were dissolved in 12 μL sample solvent (5% v/v ACN, 1% v/v FA), of which 5 μL where injected onto a Thermo Fisher

Scientific EASY-nLC coupled to a Q-Exactive mass spectrometer. Peptides were separated on a 12 cm, 75 μM inner diameter C18 (120 Å, 5 μm, Dr. Maisch) analytical column with an 81 min, 4-37% Buffer B gradient (95% ACN, 0.1%FA) and a flow rate of 320 μL/min. Mass spectrometric analysis of protein-protein cross-linked peptides was performed with a TOP15 method in data dependent acquisition mode. MS1 ions were recorded in the range of 350-1600 m/z at 140000 resolution. Fragmentation was generated by HCD activation (collision induced dissociation, normalized collision energy=25), and only precursor ions of charge state 3-8 were selected for fragmentation. Fragment ions were acquired in the Orbitrap at 17500 resolution. Dynamic exclusion was set at 20 seconds.

Identification of crosslinks with pLink was performed as published previously (Yang et al., 2012), with the following parameters: carbamidomethylation of cysteine, fixed; methionine oxidation, variable, FDR=5%. Spectra were searched against a forward and reverse database containing the UNIPROT sequences of the protein complex components.

Multiple sequence alignment of CRM1 orthologs

The amino acid sequences of 16 CRM1 orthologs (*Homo sapiens, Saccharomyces cervisiae, Trypanosoma cruzi, Schizosaccharomyces pombe, Rattus norvegicus, Mus musculus, Drosophila melanogaster, Candida albicans, Trypanosoma brucei, Dictyostelium discoideum, Xenopus laevis, Bos taurus, Aspergillus terreus, Pan troglodytes, Danio rerio* and *Chaetomium thermophilum)* were aligned with ClustalW2 (Larkin et al., 2007). The alignment was used in Chimera (Pettersen et al., 2004) to color CRM1 residues of the CRM1-SPN1-RanGTP-$_{MBP}$Nup214 complex according to their level of conservation.

Supplemental References

Adams, P.D., Afonine, P.V., Bunkoczi, G., Chen, V.B., Davis, I.W., Echols, N., Headd, J.J., Hung, L.W., Kapral, G.J., Grosse-Kunstleve, R.W., et al. (2010). PHENIX: a comprehensive Python-based system for macromolecular structure solution. Acta crystallographica. Section D, Biological crystallography 66, 213-221.

Arnold, M., Nath, A., Hauber, J., and Kehlenbach, R.H. (2006). Multiple importins function as nuclear transport receptors for the Rev protein of human immunodeficiency virus type 1. J. Biol. Chem. 281, 20883-20890.

Baake, M., Doenecke, D., and Albig, W. (2001). Characterisation of nuclear localisation signals of the four human core histones. J Cell Biochem 81, 333-346.

Brünger, A.T. (2007). Version 1.2 of the Crystallography and NMR system. Nat Prot 2, 2728-2733.

Chi, N.C., Adam, E.J.H., and Adam, S.A. (1997). Different binding domains for Ran-GTP and Ran-GDP/RanBP1 on nuclear import factor p97. J Biol Chem 272, 6818-6822.

De, I., Bessonov, S., Hofele, R., dos Santos, K., Will, C.L., Urlaub, H., Lührmann, R., and Pena, V. (2015). The RNA helicase Aquarius exhibits structural adaptations mediating its recruitment to spliceosomes. Nat. Struct. Mol. Biol. 22, 138-144.

Dolker, N., Blanchet, C.E., Voss, B., Haselbach, D., Kappel, C., Monecke, T., Svergun, D.I., Stark, H., Ficner, R., Zachariae, U., et al. (2013). Structural Determinants and Mechanism of Mammalian CRM1 Allostery. Structure 21, 1350-1360.

Emsley, P., Lohkamp, B., Scott, W.G., and Cowtan, K. (2010). Features and development of Coot. Acta crystallographica. Section D, Biological crystallography 66, 486-501.

Guan, T., Kehlenbach, R.H., Schirmer, E.C., Kehlenbach, A., Fan, F., Clurman, B.E., Arnheim, N., and Gerace, L. (2000). Nup50, a nucleoplasmically oriented nucleoporin with a role in nuclear protein export. Mol. Cell Biol. 20, 5619-5630.

Jäkel, S., and Görlich, D. (1998). Importin beta, transportin, RanBP5 and RanBP7 mediate nuclear import of ribosomal proteins in mammalian cells. EMBO J. 17, 4491-4502.

Kabsch, W. (2010). Xds. Acta crystallographica. Section D, Biol Crystal. 66, 125-132.

Larkin, M.A., Blackshields, G., Brown, N.P., Chenna, R., McGettigan, P.A., McWilliam, H., Valentin, F., Wallace, I.M., Wilm, A., Lopez, R., et al. (2007). Clustal W and Clustal X version 2.0. Bioinformatics 23, 2947-2948.

Leitner, A., Reischl, R., Walzthoeni, T., Herzog, F., Bohn, S., Forster, F., and Aebersold, R. (2012). Expanding the chemical cross-linking toolbox by the use of multiple proteases and enrichment by size exclusion chromatography. Mol Cell Proteomics 11, M111 014126.

Mahajan, R., Delphin, C., Guan, T., Gerace, L., and Melchior, F. (1997). A small ubiquitin-related polypeptide involved in targeting RanGAP1 to nuclear pore complex protein RanBP2. Cell 88, 97-107.

McCoy, A.J., Grosse-Kunstleve, R.W., Adams, P.D., Winn, M.D., Storoni, L.C., and Read, R.J. (2007). Phaser crystallographic software. J Appl Crystall. 40, 658-674.

Melchior, F., Sweet, D.J., and Gerace, L. (1995). Analysis of Ran/TC4 function in nuclear protein import. Methods Enzymol. 257, 279-291.

Mingot, J.M., Kostka, S., Kraft, R., Hartmann, E., and Görlich, D. (2001). Importin 13: a novel mediator of nuclear import and export. Embo J. 20, 3685-3694.

Monecke, T., Güttler, T., Neumann, P., Dickmanns, A., Görlich, D., and Ficner, R. (2009). Crystal structure of the nuclear export receptor CRM1 in complex with Snurportin1 and RanGTP. Science. 324, 1087-1091. .

Mueller, U., Darowski, N., Fuchs, M.R., Forster, R., Hellmig, M., Paithankar, K.S., Puhringer, S., Steffien, M., Zocher, G., and Weiss, M.S. (2012). J Synchr Rad. 19, 442-449.

Pettersen, E.F., Goddard, T.D., Huang, C.C., Couch, G.S., Greenblatt, D.M., Meng, E.C., and Ferrin, T.E. (2004). UCSF Chimera - a visualization system for exploratory research and analysis. Journal of computational chemistry 25, 1605-1612.

Quiocho, F.A., Spurlino, J.C., and Rodseth, L.E. (1997). Extensive features of tight oligosaccharide binding revealed in high-resolution structures of the maltodextrin transport/chemosensory receptor. Structure 5, 997-1015.

Roloff, S., Spillner, C., and Kehlenbach, R.H. (2013). Several Phenylalanine-Glycine Motives in the Nucleoporin Nup214 Are Essential for Binding of the Nuclear Export Receptor CRM1. J Biol Chem 288, 3952-3963.

Smyth, D.R., Mrozkiewicz, M.K., McGrath, W.J., Listwan, P., and Kobe, B. (2003). Crystal structures of fusion proteins with large-affinity tags. Protein science : a publication of the Protein Society 12, 1313-1322.

Strasser, A., Dickmanns, A., Schmidt, U., Penka, E., Urlaub, H., Sekine, M., Lührmann, R., and Ficner, R. (2004). Purification, crystallization and preliminary crystallographic data of the m3G cap-binding domain of human snRNP import factor snurportin 1. Acta Crystallogr D Biol Crystallogr. 60, 1628-1631.

Waldmann, I., Spillner, C., and Kehlenbach, R.H. (2012). The nucleoporin-like protein NLP1 (hCG1) promotes CRM1-dependent nuclear protein export. J. Cell Science 125, 144-154. .

Yang, B., Wu, Y.J., Zhu, M., Fan, S.B., Lin, J., Zhang, K., Li, S., Chi, H., Li, Y.X., Chen, H.F., et al. (2012). Identification of cross-linked peptides from complex samples. Nature methods 9, 904-906.